Reheating Quenching And Partitioning Microstructures To Modify Phase Fractions

Master Thesis

To complete Materials Science and Engineering master programm
Faculty of Mechanical, Maritime, and Materials Engineering (3ME)
TU Delft

Muhammad Fakhry Hatta
August 2018

This thesis is dedicated to
my beloved wife Nida and
our happy girl Aurora

Reheating Quenching and Partitioning Microstructures to Modify Phase Fractions

By

Muhammad Fakhry Hatta

in partial fulfilment of the requirements for the degree of

Master of Science

in Materials Science and Engineering

at the Delft University of Technology,

to be defended publicly on Thursday August 30, 2018 at 09:00 AM.

Supervisor:	Prof. dr. Maria J. Santofimia	
	Sudhindra Ayenampudi, M.Sc.	
Thesis committee:	Prof. dr. Maria J. Santofimia	TU Delft
	Dr. Vera Popovich	TU Delft
	Dr. Carola A. Celeda Casero	TU Delft

Acknowledgement

All praise is due to Allah, the Lord of the Universe; The Beneficent, The Merciful. *Shalawat* and *salam* upon prophet Muhammad peace be upon him.

There are no such things like coincidence in life because every path in life is indeed full of lesson-learned and unveil meaning including my master study journey at Technische Universiteit Delft, The Netherlands. In this short section I would like to express my gratitude to all who support me morally, technically, and academically.

First of all, I would like to acknowledge my sponsor Indonesian Endowment Fund for Education (LPDP) which gave me opportunity to pursue master degree at TU Delft. I can learn many things in Delft not only deepen my Materials Science knowledge but also strengthen my character in the global, diverse, and competitive environment.

I would like to express my wholeheartedly gratitude to my supervisors: Prof. Maria Jesus Santofimia Navarro and Sudhindra Ayenampudi for the guidance, patience, and support during since the beginning of this work. Our fortnightly meetings were always somehow scary but at the same time is also encouraging. Maria always patiently guided me with her critical questions. I found it very hard to follow at the beginning but gratefully I survived and definitely will missed that enlighten meetings in the future. On the other hand, Sudhindra always support me with his warm and friendly suggestion. His detailed suggestion made me always want to give the best of my work. I am very blissful for the opportunity working with them. I also want to thank Dr. Vera Popovich for being the committe member.

This work will not finish without contribution of the technicians in the Materials Science Department. I would like to say thank you to Nico Geerlofs who trained me conducting dilatometry experiments, Richard Huizenga who carried out the XRD experiment of my samples, Kees Kwakernaak who trained me operating SEM so I can captured the beautiful microstructure of my samples, Sander van Asperen who gave me valuable input during sample preparation, and Elise Reinton who taught me how to run the micro hardness test.

I would also say thank you to my former lecture at Institut Technology Bandung, Indonesia especially to Dr. Ir. Arif Basuki and Dr. Ir. Adityanto Ramelan, who gave me support to continue study in materials science area and convinced me to pursue it at TU Delft. I definitely have no regret for following your suggestion indeed the decision was truly right.

My warmest and sincerest gratitude is for my family. Thanks to my lovely wife for your endless love and support, my solehah girl Aurora who always gave me smile (and sometimes tears) every day, my family in Bandung and Pangkep for the continuous prayer and support which made me believe that I could finish my study.

Nevertheless, I want to thank to all my materials science mate, all Indonesian student in Delft, Keluarga Muslim Delft, and all colleague all over the Netherlands for the togetherness and joy we shared with.

Delft, 06 August 2018

Muhammad Fakhry Hatta

Abstract

The Quenching and Partitioning (Q&P) process starts with an austenitization process followed by rapid cooling to a temperature named quenching temperature ranged between the martensite start (M_s) and martensite finish (M_f) temperatures to establish initial fractions of martensite and austenite. Afterwards, the material is reheated to a particular partitioning temperature and for a given time to allow the carbon diffusion from martensite to austenite. Finally, the steel is quenched to room temperature and a fraction of fresh untempered martensite may form from the least stable austenite. The whole process determines the phase fraction of the constituent phases, namely: tempered martensite (M_1), retained austenite, and un-tempered martensite (M_2). This combination of phases has the potential to simultaneously improve strength and elongation of steels due to their small grain sizes and the transformation-induced plasticity resulting of the transformation of the retained austenite into martensite during a deformation.

It is known that the fraction of retained austenite of Q&P steels depends on the quenching temperature, showing a bell-like relation. The volume fraction of retained austenite shows a maximum at a particular quenching temperature somewhat intermediate between the M_s and M_f temperatures, known as the optimum quenching temperature, below and upper which the volume fraction of retained austenite decreases in either way.

Recently, it is reported [1] that retained austenite fraction after reheating up to 700ºC followed by quench losses its dependency of quenching temperature and reaches a constant value. This can be a manner to further control phase fractions and consequently the mechanical properties of Q&P steels. The mechanisms by which the volume fraction of austenite changes to reach that constant value are not well understood and are the focus of the present study.

In the present work, Q&P samples with chemical composition 0.31C-4.58Mn-1.52Si (wt.%) were reheated up to 700ºC and quenched directly to compare the retained austenite fractions of reheated and un-reheated (Q&P) samples. It was found that the retained austenite fractions tend to have a constant value after reheating to 700ºC followed by quenching, whereas the retained austenite fraction of the Q&P samples showed an optimum value and usual dependency with quenching temperature. It was also observed that the highest and lowest drop of retained austenite occurred in the reheated Q&P samples at 160ºC and 80ºC of quenching temperature. These samples were reheated to 900ºC to have a complete observation of microstructural events by means of dilatometry, optical and electron scanning microscopy, hardness, and X-Ray diffraction measurement.

Interrupted reheating was applied to understand the microstructural changes during reheating. The two samples were interruptedly reheated and directly quenched at 450ºC, 530ºC, 610ºC, 720ºC, and 740ºC to measure the retained austenite fraction and to capture the corresponding microstructure around the observed changes in slope. The retained austenite fractions evolution of both samples were measured and compared. It was found that the decreasing of retained austenite fraction started around the critical temperature of 600ºC and remained up to 700ºC of reheating temperature. Further reheating process increased the retained austenite fraction.

In the specimen showing the lowest drop of retained austenite fraction, retained austenite decomposed by two mechanisms. The first one was the formation of discrete particles of cementite, which originally came from film type austenite. The second was the formation of globular carbides within tempered martensite. On the other hand, river-like patterns were observed surrounding the martensite region. The river-like patterns mainly consist of martensite from new austenite that formed between 720ºC and 750ºC.

In the highest drop of retained austenite fraction sample, retained austenite decomposed by three mechanisms. The first two mechanisms were similar to the previous sample. The last mechanism was the formation of substructure within Martensite-Austenite islands. River-like patterns were also observed surrounding the martensite region, consisting of martensite which originally came from new austenite as a product of (martensite and) carbide transformation that formed between 720ºC and 745ºC and lath martensite which originally came from the unstable austenite forming upon reheating to 740ºC.

Table of Content

Chapter 1: Introduction

The requirement of environmental friendly materials is getting more critical. Pacts and agreements, such as Paris agreement (officially called United Nation Framework Convention on Climate Change), motivated many countries and indirectly also industries to adjust their environmental policies by either replacing hazardous substances or reducing the weight of the applied materials without sacrificing its quality.

This requirement is also faced by steel industry, especially in the automotive sector. For decades, advanced high strength steels (AHSS) have been massively studied. A summary of the developed steels as a function of the strength-ductility is shown in Figure 1. The figure displays commercial and concepted steel, including various types of AHSS. The first generation of AHSS consists of Dual Phase (DP) steels, Complex Phase (CP), Transformation Induced Plasticity (TRIP) steels, and Martensitic Steel (MS), whereas the Twinning Induced Plasticity (TWIP) steel is referred to the second generation of AHSS. The third generation of AHSS is expected to have higher strength combined with relatively similar ductility than the first generation of AHSS, but it is expected to lead to lower production costs than TWIP steel [2]

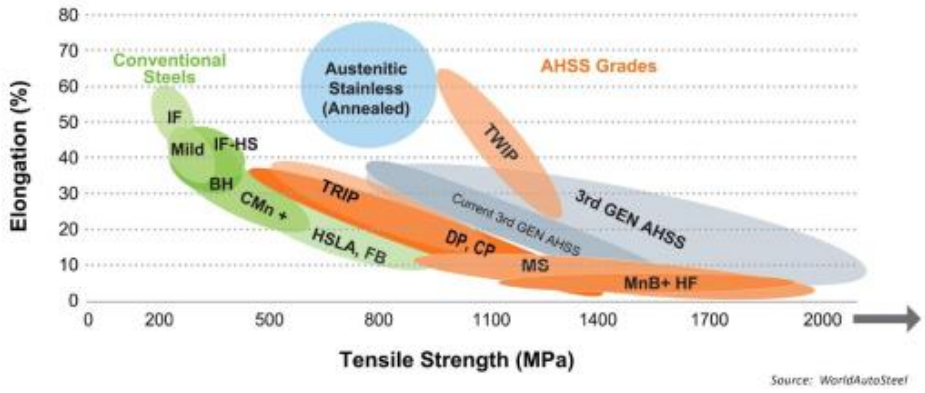

Figure 1 Steel development w.r.t its strength and ductility [3]

1.1 Quenching and Partitioning (Q&P) process

In order to achieve a successful third generation of AHSS, Speer and coworkers [4] [5] developed the quenching and partitioning (Q&P) process. This process can increase the fraction and stability of retained austenite (RA), which contributes to the ductility of the steel, while remaining martensite contributes to the strength.

The Q&P process starts with austenitization to either the intercritical or fully austenitic region. Then the sample is quenched to a temperature named “quenching temperature” (QT) which is between the

martensite start temperature (M_s) and above the martensite finish temperature (M_f). The process continues by heating up the sample to a particular partitioning temperature (PT) at which the material is isothermally held during a certain partitioning time in order to allow the carbon diffusion from martensite into austenite. Finally, the process is ended by quenching the samples to room temperature (RT). Figure 2 Overview of the Q&P process .

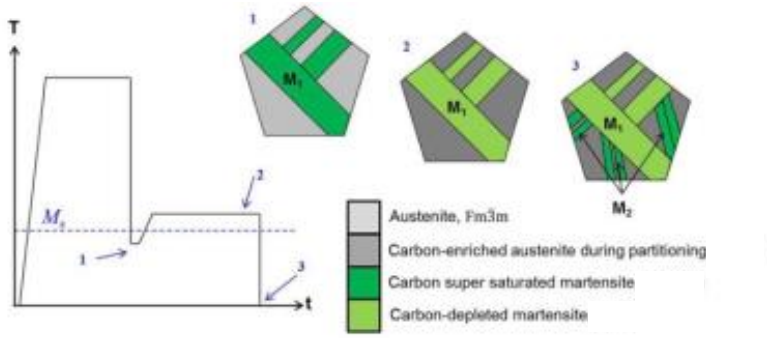

Figure 2 Overview of the Q&P process [6]

The microstructure of Q&P steels is influenced by the process parameters. If the fully austenitic condition is preferred, as will be considered in the present work, the microstructure consisted of tempered martensite (M_1), retained austenite, and untempered martensite (M_2) [6]. M_1 is the generated martensite upon first quenching and will be carbon depleted as it is tempered at the partitioning stage. The fraction of M_1 is controlled through the selected quenching temperature. Retained austenite is the austenite that remains after the Q&P process at room temperature. M_2 is the martensite that is formed after the second quenching to room temperature, which inherits the high carbon content from its parent phase (carbon-enriched austenite) [6].

In Q&P steels, there is an optimum quenching temperature somewhere between the M_s and M_f leading to a maximum fraction of retained austenite that can be predicted [5] [7]. Quenching above the optimum quenching temperature will produce a too small fraction of M_1 which will lead to low carbon partitioning to austenite. Therefore, not all austenite will remain retained after the final quenching. In contrast, quenching below the optimum quenching temperature will produce too much martensite which contained carbon greater than needed to stabilize austenite to room temperature [5].

Figure 3 shows an example of how the optimum quenching temperature is predicted in an alloy with 0.19C-1.69Mn-1.63Si (wt.%) of chemical composition, in which the partitioning temperature is fixed to 400^{o}C, and various quenching temperatures and partitioning times are considered. The solid line corresponds to retained austenite fractions as a function of the quenching temperature assuming complete partitioning, whereas the points correspond to retained austenite fractions as a function of quenching temperature considering the kinetics of carbon partitioning. The optimum quenching temperature in the former case is at 240^{o}C of quenching temperature and produced 18% of retained

austenite. In the latter case, the precise partitioning time needs to be chosen to acquire the same optimum quenching temperature. It gives the general idea of how important the process parameters are during the Q&P process.

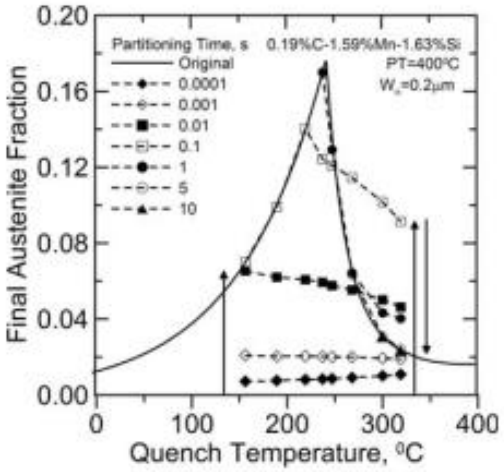

Figure 3 The fraction of retained austenite as a function of the quenching temperature. The composition of the steel and the heat treatment parameters are indicated on the figure [7]

The partitioning of carbon from martensite to austenite is governed by the carbon-constrained equilibrium (CCE) condition ([4] [8]). CCE has two key assumptions [4]. First, the diffusion of carbon is considered complete when the chemical potential of carbon in austenite and ferrite are the same. This condition is contrasted with the paraequilibrium condition where both chemical potentials of carbon and iron are the same (Figure 4). Second, the substitutional atoms are conserved in both phases to support a fix martensite/austenite interface.

It was later proposed that the martensite/austenite interface can also migrate. Thus, the austenite fraction after partitioning can be different from the austenite fraction after first quenching [9]. The migrated interface can be calculated and it is found that the interface`s movement can take place in either direction. [10].

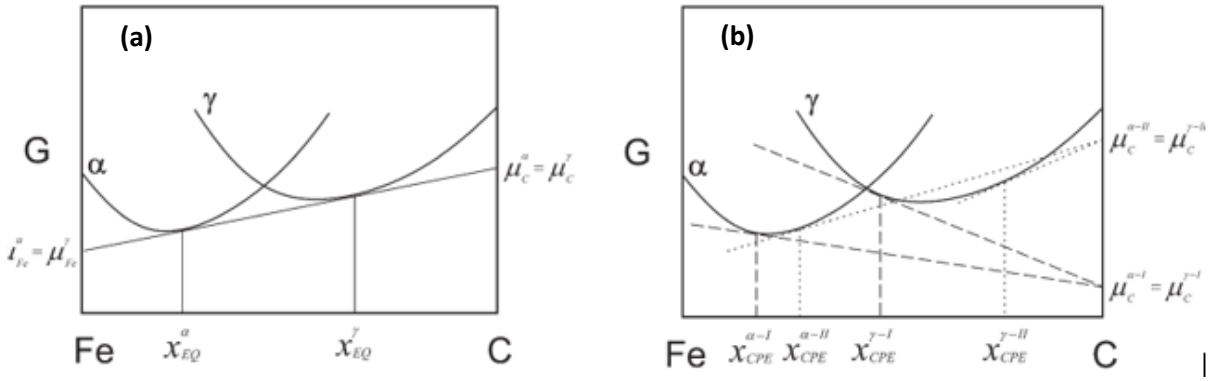

Figure 4 Paraequilibrium (a) and CCE (b) condition. X is carbon fraction, EQ is equilibrium, and μ is chemical potential [4]

During the Q&P process, other competing reactions such as carbides formation and bainite formation need to be avoided [11] [10]**.** In order to achieve the last condition, alloying elements such as manganese, nickel, and chromium are added to retard bainite and ferrite formation [12] while silicon and aluminium are used to suppress carbides formation that can consume carbon during partitioning process [5]. Recent investigations found that even though Si is added to the steel alloy, formation of carbides can still occur [6]

The mechanical and thermal stability of retained austenite is crucial for Q&P steels. The mechanical stability of the retained austenite is the resistance of the austenite to transform into martensite during application of a deformation. It has been reported that the fraction and carbon concentration of the retained austenite are decisive factors controlling the mechanical stability [13] [14]. The thermal stability of retained austenite is defined as the resistance of the austenite against transformation into stable phases, like cementite and ferrite or into metastable phase, like martensite phases. It is reported that thermal stability of retained austenite is highly influenced by the carbon content in the austenite grain, austenite grain size and dislocation density [15].

Koopmans [1] applied a Q&P process to an alloy with the chemical composition of 0.2C-3.51Mn-1.525Si (wt.%) considering various quenching temperatures (140-340ºC) and a fix partitioning temperature and time (400ºC and 50 s). The process led to the generation of different retained austenite fraction as shown by black dots in Figure 5. In order to study the thermal stability of retained austenite, the same alloy was subjected to the Q&P process, subsequently reheated up to 700ºC with 5 ºC/minute of heating rate, and followed by quenching to room temperature. The retained austenite fractions of reheated samples were measured and are shown as red dots in Figure 5.

The results of retained austenite fractions measurements in the Q&P and reheated specimens were divided into three regions. In the region I, the retained austenite fractions increased after the reheating process followed by direct quenching. In the region II, the retained austenite fractions converged into a

constant value regardless of its quenching temperature after reheating to 700°C followed by quench (red dots). In the region III, the retained austenite fractions decreased after the reheating process followed by direct quenching.

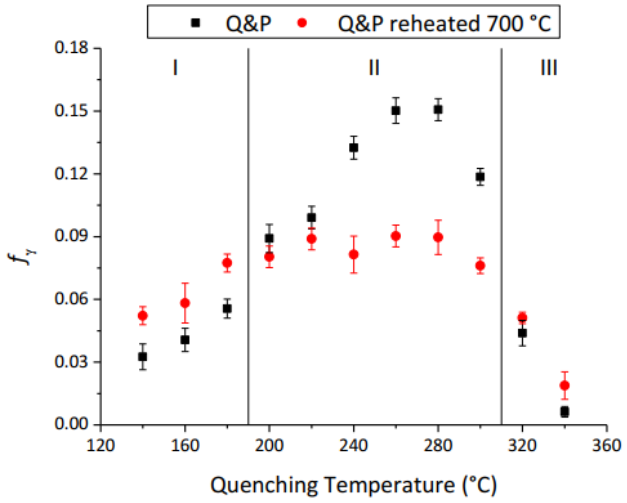

Figure 5 The fraction of retained austenite in QP steel w.r.t its quench temperature. The legend is indicated in the picture [1]

1.2 Tempering of steels

In the following, the different microstructural changes taking place in martensite during heating will be explained by dividing them into stages as the tempering temperature increases [1] [16] [17] [18] [19] [20] [21]. Indicated temperatures per stage may change with heating rate and composition. Furthermore, some of these stages may occur simultaneously.

- Stage 1 : Carbon segregation (-40-100°C) [17]

  Carbon atoms are redistributed to low energy sites due to its high mobility. Dislocations, vacancies, and lath boundaries of martensite are examples of the preferred place to diffuse. The carbon segregate either as clusters, modulated clusters on specific martensite planes or long period arrays of carbon. The activation energy for carbon segregation is 67-91 kJ/mol [22].
- Stage 2 : Formation of transition carbides (100-250°C)

  Typically, the transition carbides are fine having approximately 3-5 nm in size and placed within the martensite matrix. It is differentiated based on its crystal structure. The epsilon carbide is the transition carbides with hexagonal close-packed structure. Another type of the transition carbides is eta carbide which has orthorhombic crystal structure [16]. Figure 6 shows the eta carbide in a quenched and tempering steel. The activation energy for the formation of transition carbides is 102-135 kJ/mol. [22]

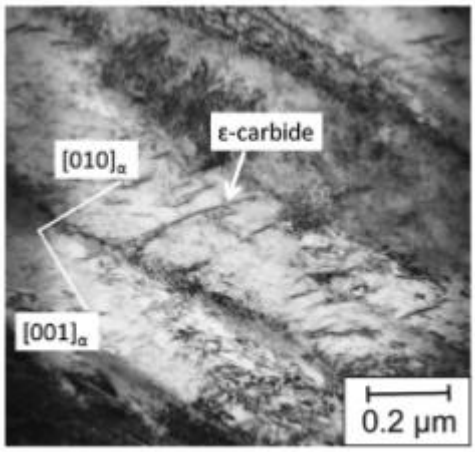

Figure 6 Eta carbide presence after tempering [18]

- Stage 3 : Retained austenite decomposition

  The retained austenite decomposition occurs after the transition carbides formation is finished [17] [16]. After the Q&P process, it is reported that low carbon and high carbon retained austenite are observed. The low carbon retained austenite will decomposed into (bainitic) ferrite and cementite (at 250-370ºC), whereas the high carbon retained austenite decomposed into ferrite and cementite at higher temperature (at 500-600ºC) [1]. In addition, the film like retained austenite can decompose into discrete particles of cementite (Figure 7). The activation energy for retained austenite decomposition is 174-221 kJ/mol [22].

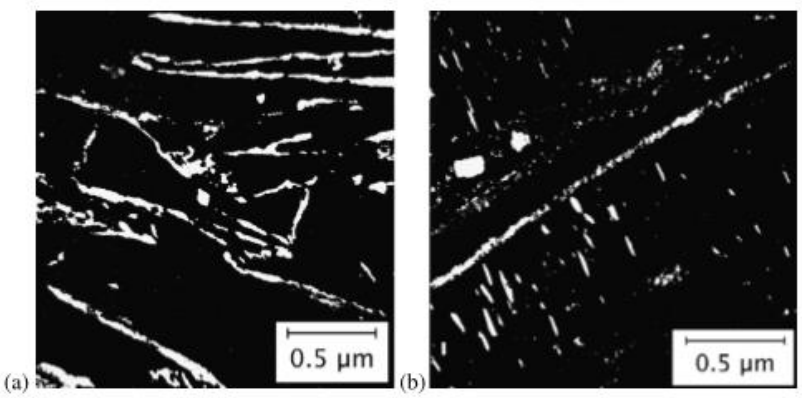

Figure 7 Dark field transmission electron micrograph (a) as quenched condition. The film like retained austenite is between the martensite plates (b) the retained austenite is decomposed into discrete particles [18]

- Stage 4 : Replacement of transition carbides

  At elevated temperature, the mentioned transition carbides are replaced by chi carbides but it will subsequently transform into theta carbides (cementite, Fe_3C) which have orthorhombic crystal structure [16]. The cementite preferred site to nucleate are at the former transition carbides, twin boundaries, martensite lath boundaries and martensite lath interface (Figure 8) [18]. The activation energy for cementite formation is 225 kJ/mol [22].

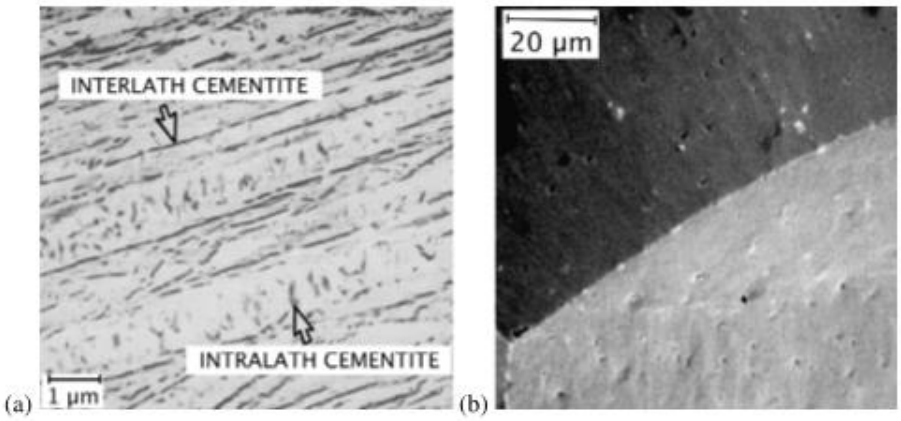

Figure 8 (a) interlath and intralath cementite (b) cementite formed at the prior grain boundaries [18]

- Stage 5 : Spheroidization of carbides [18]

  As the tempering goes to higher temperature, the cementite will coarsen and finally spheroidize at approximately up to 650^{o}C (Figure 9). At this stage, the carbon content in martensite will drop significantly and martensite losses tetragonality. Eventually, martensite will be replaced by more equiaxed ferrite. The spheroidized cementite will be found within the ferrite matrix.

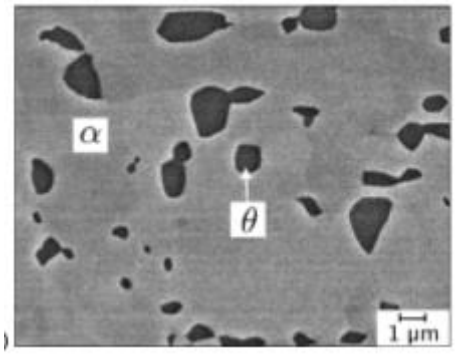

Figure 9 Spheroidized cementite observed within ferrite phase. It is observed after tempering at 650^{o}C for 1.5 hours [18]

- Stage 6 : Recovery and recrystallization

  Recovery is defined as a process to reduce internal stored energy by rearranging or annihilating defects, such as dislocation, in the crystal structure. Normally, these defects are generated from deformation processes subjected to the metals. Recovery can occur at 400^{o}C of tempering temperature. This often overlap with the recrystallization process which replaces the deformed grains with defect free new grains and occurs between 600-700^{o}C.

- Stage 7 : Martensite reversion

  As the steels are further reheated, the A_{c1} temperature can be crossed. Under this condition, the martensite will revert into (equiaxed) ferrite and it will progressively transform to austenite following the equilibrium phase diagram.. The reversion will end after the samples are reheated passing the Ac_3 temperature.

1.3 Research questions

The fraction of retained austenite in Q&P steels is related to the quenching temperature. It showed an optimum value at particular quenching temperature below and upper which it decreases in either way. It is reported that the retained austenite fraction of the Q&P steels tended to lose its dependency on quenching temperature and to have a constant value after reheating at 700ºC followed by direct quenching. Nevertheless, the mechanisms that governed the changes in the fraction of retained austenite are still unexplained.

In this thesis, the mentioned phenomena are discussed by considering the following research question:

- What are the microstructural changes encountered by a Q&P microstructure during reheating to the fully austenitic region?

1.4 Approach

This work is divided into the following steps:

- The generation of the Q&P microstructures applying various quenching temperatures and fixed partitioning conditions. The related fraction of constituents phases are calculated
- The reheating the Q&P samples up to 700ºC. The fraction of retained austenite is measured and compared with the rest of Q&P samples.
- The samples with highest and lowest drop of retained austenite fraction are chosen to be reheated up to 900ºC in order to fully capture the microstructure events during reheating to the fully austenitic region
- The application of interrupted reheating processes at different temperatures around the observed thermal expansion or contraction in dilatometry curve, following by the analysis of the corresponding microstructures.

Both the Q&P treatments and reheating processes are conducted in the dilatometer to generate and study the microstructural evolution of the steel. The microstructural events are analyzed using the dilatometry curves and their derivative curves. Dilatometry and X-ray diffraction measurements are used to quantify the constituent phases of the Q&P steel. The microstructure of the samples is observed by Scanning Electron Microscopy and Optical Microscopy. Furthermore, hardness tests was applied to the selected samples in order to verify the phases within the microstructures.

Chapter 2: Materials and experimental methods

This chapter contains information about the materials, the sample preparation, and the methods, namely: Dilatometry, X-Ray Diffraction, Optical Microscopy (OM), and Scanning Electron Microscopy (SEM).

2.1 Material

2.1.1 Chemical composition

The material used in this research is a steel designed for Q&P heat treatments with the chemical composition shown in Table 1. The steel was forged during its processing. The as-forged samples were produced at the RWTH Aachen.

Table 1 Chemical composition of the Q&P steel (wt. %)

C	Mn	Si	Mo	Al	Ni	Cr	P
0.31	4.58	1.52	<0.005	0.01	<0.01	0.002	0.14

From the chemical composition, it can be seen that the Q&P steel is a medium carbon steel (0.30-0.60 wt. %), based on the American Iron and Steel Institute (AISI) and Society of Automotive engineering (SAE) classification [23]. It contains high content of Mn and Si in order to suppress the competing reaction such as bainite during the application of the Q&P process and to hinder the carbide precipitation, respectively [24].

2.1.2 Q&P steel microstructures

Microstructural banding is commonly observed in Q&P steels. It is due to the high content of manganese expelled into interdendritic region during solidification. Actually, manganese has higher value of equilibrium partition ratio k (0.79) compare to phosphorous (0.14), for example. Lower k value means the solutes are likely to segregate. The amount of solutes are also considered a determine factor [25]. As it can be seen in Table 1, the amount of Mn outnumbered P in the Q&P steel. As expected from the high Mn content, microstructural bands are observed in the Q&P steel. The bands are more clear when the samples are quenched near M_s temperature. 200^{o}C for instance.

The typical microstructure of Q&P steel consists of the combination of dark and light regions after etching and observing with optical microscopy. Based on the etching theory [26], it is known that the appeared (dark) phases are resulted from the selective corrosion of the anodic part with respect to cathodic part (light region meaning not reacted with the etchant). The used etchant (2 % nital) is the common solution to reveal the steel microstructure containing ferrite (BCC) mainly. Thus, the dark region on the Q&P microstructure can be correlated with the BCC phases, namely ferrite, bainite (ferrite

with interpenetrated cementite in between), and martensite (elongated BCC crystal structure). The bainite formation is hypothetically suppressed and excluded from the recognition on Q&P microstructure. Since the Q&P process involves a relatively fast cooling, ferrite presence on the microstructure become unlikely. The dark regions on the microstructure are considered as martensite, whereas the light regions are considered retained austenite or high carbon martensite expected after Q&P heat treatments.

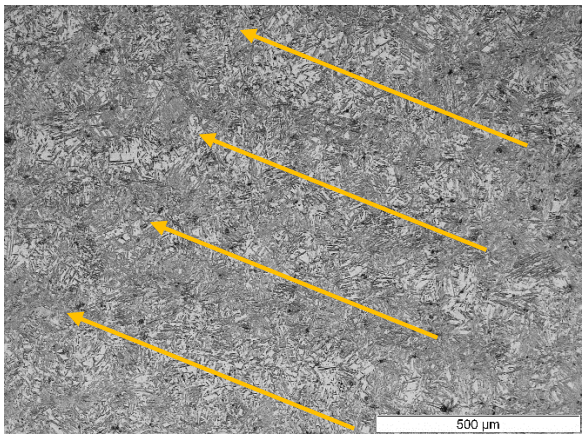

Figure 10 Microstructural bands are observed in Q&P steel (yellow arrows); quenched to 200^{0}C

2.2 Sample preparation

Throughout this study, cylinder samples are used with 10 mm in length and 4 mm in diameter. The cylinder samples will be used sequentially on different experiments. First, the designed heat treatment is applied with dilatometry. Before putting the specimen in the dilatometer, the samples are surface ground with a 800 grit SiC paper in order to remove the oxide formed in the surface, followed by ultrasonic cleaning in ethanol for five minutes. Next experiment is the X-ray diffraction measurement. The samples are cut into half in the Struers Minitom with a diamond grinding disc (Struers M1D10) and subjected to the metallography procedure, namely: grinding with SiC paper from 800 to 2000 grit sequentially, and polishing with 3 and 1 µm diamond paste. Re-polishing and etching with 2% nital are necessary in order to take the microstructure of the samples either with OM or SEM.

The samples are named indicating the combination of their quenching temperature and reheating temperature (R). For example:

1. Sample only subjected to Q&P route will be named QPXXX, which XXX refers to the quenching temperature.
2. Sample that is subjected to Q&P and reheating processes will be named QPXXXRYYY which XXX refers to the quenching temperature and YYY refers to the reheating temperature.

2.3 Dilatometry

2.3.1 Description

Dilatometry is a powerful device to track the microstructural events during a heat treatment by recording the length change of the specimens as a function of temperature and time. The mentioned microstructural events are characterized by deviations on the either thermal expansion or contraction in the dilatometry curve.

Schematically (Figure 11), the dilatometry contains two quartz push rod for clamping the sample and a Linear Variable Differential Transformer (LVDT) for recording the length change. A thermocouple is spot welded on the sample and used to record the temperature. Cooling is using Helium gas, whereas heating is using an induction coil.

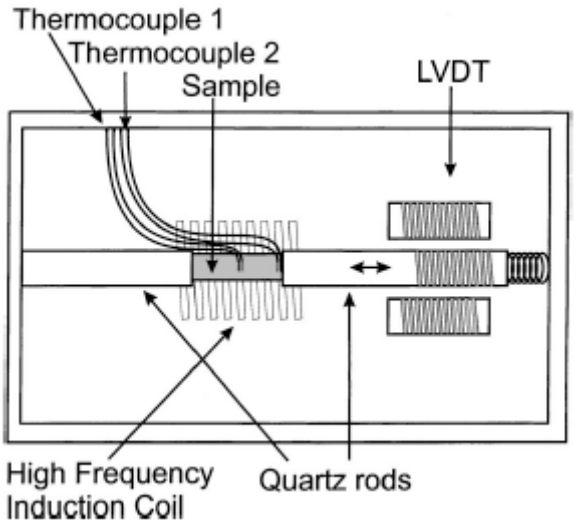

Figure 11 Schematic overview of dilatometry machine [27]

2.3.2 Dilatometry curve

The output data of the dilatometer measurement can be presented by showing the length change $\frac{\Delta l}{l_o}$ as a function of temperature on heating or cooling, where l_o is the initial length of dilatometer specimen and l is the measured length at specific temperature of the dilatometry sample. Another way to present the data is by plotting the derivative of the length change $\frac{d}{dT}\left(\frac{\Delta l}{l_o}\right)$ which give more apparent indication of the microstructural events happening during heating or cooling. Figure 12 shows the comparison between the two mentioned methods. In the dilatometry curve, the thermal expansion or contraction change of linearity can be observed visually on the curve (red arrows). On the other hand, the

microstructural events in the derivative of dilatometry curve are indicated by the either the peaks or valleys (orange arrows) while the range of linear derivative means no phase transformation.

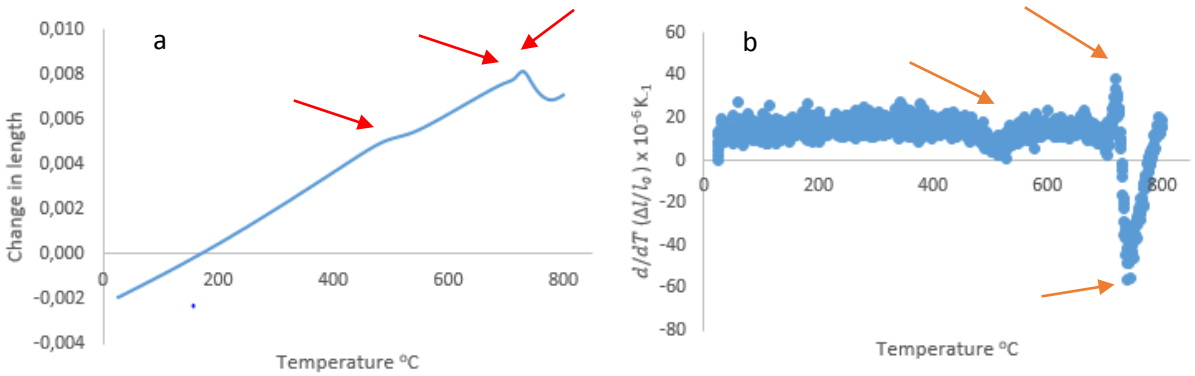

Figure 12 Comparison between (a) change in length $\frac{\Delta l}{l_o}$ during reheating up to 800°C with heating rate of 5°C/s (b) corresponding derivative of (a) $\frac{d}{dT}\left(\frac{\Delta l}{l_o}\right)$. Red and orange arrows indicated the microstructural events seen on the graph.

In the derivative curve, the microstructural events correspond with positive of negative peaks (Figure 13). The positive peaks are related to the microstructural events involving expansion of the samples like decomposition of the austenite and ferrite formation. In contrast, the negative correspond to microstructural events involving contraction of the samples like carbide precipitation or austenite formation.

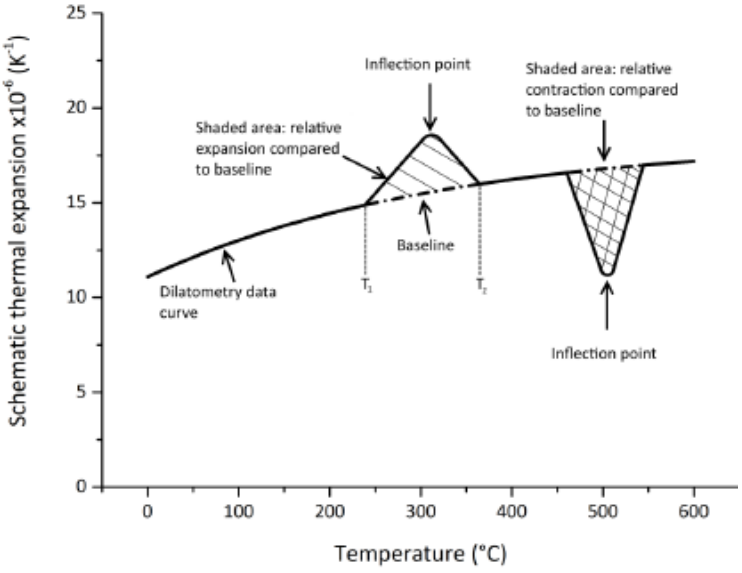

Figure 13 Schematic overview of derivative $\frac{d}{dT}\left(\frac{\Delta l}{l_o}\right)$ curve [1]

The length change due to microstructural events can be calculated from the derivative of the dilatometry curve by:

$$\left(\frac{\Delta l}{l_0}\right)p = \int_{T_1}^{T_2} \alpha_{exp}\, dT - \int_{T_1}^{T_2} \alpha_b\, dT \quad (2.10)$$

where $\left(\frac{\Delta l}{l_0}\right)p$ is the length change related to the microstructural events observed in the derivative curve, T_1 and T_2 are at the temperature which the microstructural events start and end, respectively, α_{exp} and α_b are the derivative $\frac{d}{dT}\left(\frac{\Delta l}{l_o}\right)$ of the experiment and baseline (Figure 13). The calculation of length change above is measured by appending the area under the peaks restricted with the baseline which is defined as no microstructural events taking place there.

2.3.3 Phase calculation

The dilatometry curve can give the overview of the microstructural events when the samples are subjected to the heat treatment by looking into its length change with respect to temperature, instead of the volume change. Assuming that the material follows an isotropic behavior, the relation between the length and volume change can be written as given by eq. 2.1:

$$\frac{3\Delta l}{l} \cong \frac{\Delta V}{V} \qquad (2.1)$$

where $\frac{\Delta l}{l}$ is the length change, $\frac{\Delta V}{V}$ is the volume change, V is the volume at specific temperature, and l is the length at specific temperature of the dilatometry sample. The volume change itself can be defined by the relative differences of the phase fractions and molar volume of the constituent phases before and after phase transformation (eq. 2.2)

$$\frac{\Delta V}{V} = \frac{\Sigma\, f_i^a V_i^a(T) - \Sigma\, f_i^b V_i^b(T)}{\Sigma\, f_i^b V_i^b(T)} \qquad (2.2)$$

where f_i is the molar fraction of the phase i and $V_i(T)$ is the atomic volume of the phase i at certain temperature (T), whereas a and b correspond to the before and after phase transformation.

In order to get the phase fraction, the atomic volume needs to be known. The atomic volume can be calculated by:

$$V_i = \frac{a_i b_i c_i}{N_i} \qquad (2.3)$$

$$V_i = \frac{(a_i)^3}{N_i} \qquad (2.4)$$

where a_i, b_i, c_i are the lattice parameters of the phase i measured in X-ray diffraction at room temperature and N_i is number of atoms in an unit cell of the crystal structure. Eq. 2.3 is for the orthorhombic crystal structure, whereas eq. 2.4 is for cubic crystal structure. The atomic volume at high temperature can be calculated involving the thermal expansion of the respected phases (eq. 2.5 and 2.6).

$$V_i(T) = \frac{a_i^T b_i^T c_i^T}{N_i} = \frac{a_i b_i c_i}{N_i}.\left(1 + 3.\beta_i(T - T_0)\right) \quad (2.5)$$

$$V_i(T) = \frac{\left(a_i^T\right)^3}{N_i} = \frac{(a_i)^3}{N_i}.\left(1 + 3.\beta_i(T - T_0)\right) \quad (2.6)$$

where $a_i^T b_i^T c_i^T$ and β_i are the lattice parameters and thermal expansion coefficient of the phases i at T temperature, whereas T_0 correspond to the temperature which the lattice parameters are calculated, in this case at room temperature. The relevant crystallographic data can be seen in Table 2

Table 2 Relevant crystallographic data for iron phases [28]

Phase	**Lattice parameter (Å)**	**β_I (K^{-1})**	**N_i**
BCC α-Fe	a= 2.8664	1.244×10^{-5}	2
BCT α_M	a= 2.8664-0.014w_c c= 2.8664+0.115w_c	1.244×10^{-5}	2
FCC γ-Fe	a= 3.556+0.0453w_c	2.065×10^{-5}	4
Orthorhombic θ (Fe_3C)	a=4.5246 b=5.0885 c=6.7423	0.840×10^{-5} (at350°C)	12

It is discussed in the section 1.1, bainite often forms during the Q&P process, even though suppressing alloying element such as manganese are added. Bainite can be characterized by fine plates of ferrite organized in the form of sheaves. Depending on the isothermal transformation temperature, bainite is described into two categories, namely: upper and lower bainite. Figure 14 show the formation process of lower and upper bainite. Upper bainite is characterized by the presence of carbides between ferrite plates. The carbides precipitated originally from austenite which is enriched by carbon from supersaturated ferrite plates. If alloying elements suppressing cementite precipitation such as silicon are added to the steel, cementite does not precipitate between the bainitic ferrite plates and retained austenite in these locations is found instead. Upper bainite forms at the isothermal transformation temperature range of 400-550°C. Lower bainite is characterized by carbides within and between ferrite plates. The former precipitated from carbon enriched austenite, where the latter precipitated from the supersaturated ferrite plates. Lower bainite occurs in the transformation temperature range of 250-400°C [29]

In this study, it is assumed that only upper bainite may form during the partitioning process. It is considered as competing reaction to carbon partitioning process from martensite into retained austenite.

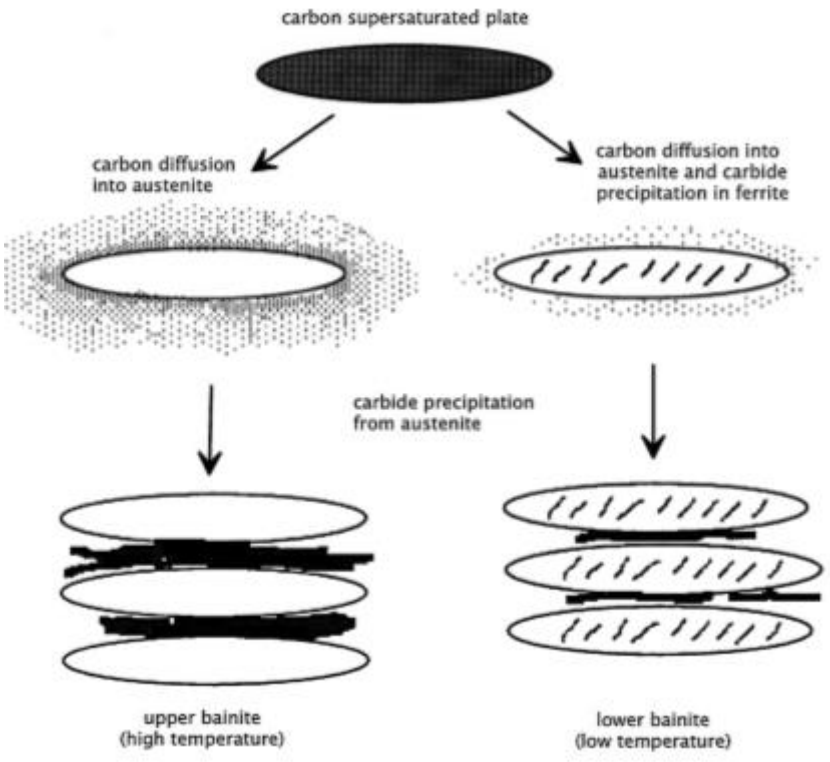

Figure 14 Schematic formation of the upper and lower bainite [29]

Upper bainite formation in the case in which cementite precipitation is suppressed can be written by the following reaction:

$$\gamma \rightarrow \alpha_b + \gamma_b$$

The bainite formation will proceed until the carbon concentration in untransformed austenite reaches the value defined by T_o curve. The molar fraction of bainitic ferrite and carbon enriched austenite can be calculated by:

$$f_{\alpha_b} = \frac{x_C^{\gamma_b} - x_C^{\gamma}}{x_C^{\gamma_b} - x_C^{\alpha_b}} f_{\gamma} \quad (2.7)$$

$$f_{\gamma_b} = \frac{x_C^{\gamma} - x_C^{\alpha_b}}{x_C^{\gamma_b} - x_C^{\alpha_b}} f_{\gamma} \quad (2.8)$$

where x_C^{γ}, $x_C^{\gamma_b}$, and $x_C^{\alpha_b}$ are carbon concentration of austenite, carbon enriched austenite, and bainitic ferrite before and after bainite formation. The relative length after bainite formation can be calculated by:

$$\frac{\Delta l}{l} = \frac{1}{3} \cdot \frac{f_{\alpha_b} V_{\alpha_b} + f_{\gamma_b} V_{\gamma_b} - f_{\gamma} V_{\gamma}}{\Sigma f_i^b V_i^b} \quad (2.9)$$

2.4 X-ray diffraction

X-ray diffraction is used to determine the phase fraction of retained austenite (f_{RA}) and its lattice parameter. After being cut and polished, the samples are placed next to each other on a Si{510} wafer. Plasticine is used to make sure that the samples provide flat surface. Furthermore, the top surface of the samples are aligned with the goniometer axis. The measurement is conducted in the Bruker D8 Advance diffractometer Bragg-Bentano geometry with graphite monochromator and Vantec position sensitive detector using Co-Kα radiation, divergence slit 6A16, V12, scatter screen 10 mm. It is operated at 45 kV and 35 mA. The sample is scanned with range of 2θ from 40-130°, step size of 0.035° 2θ, and counting time per step of 2 s. The scanned data is then analysed using Bruker software Diffrac EVA 4.2.2.

2.4.1 Phase fraction of retained austenite calculation: Jatczak method [30] [31]

In this measurement, the sample is assumed to be consisted of ferrite (which represent martensite) and austenite. The fractions of the constituent phases are obtained by comparing the area under all of one phase peaks with the total area of all phase peaks. For example: the fraction of the (retained) austenite (f_{RA}) can be calculated by appending all area under austenite peaks {110}, {200}, {211}, and {220}. The related equation is:

$$f_{RA} = \frac{I_{RA}}{I_{RA} + I_{\alpha}} \quad (2.11)$$

where I_{RA} and I_{α} is the normalized intensity of the (retained) austenite and ferrite (martensite) peaks. Those can be calculated by (I_{α} is calculated in the similar manner):

$$I_{RA} = \frac{1}{n}\sum_{i}^{n}\left(\frac{I^{*}_{RA_{hkl}}}{R_{RA_{hkl}}}\right) \quad (2.12)$$

Where *n* is the number of the retained austenite peaks, $R_{RA_{hkl}}$ is the calculated intensity of a particular {hkl} austenite peak (standard value), and $I^{*}_{RA_{hkl}}$ is the measured intensity of a particular {hkl} retained austenite peak above the background. In the calculation, the *R* value need to be corrected by multiplying with sin(θ). This is due to the fact that the received and diffracted intensity are linearly proportional with 2θ. The *R* values are taken from [31]

The {111} (retained) austenite peak is hard to append precisely since it overlaps with the {110} ferrite peak. The solution of this problem is by subtracting the total area containing both {111} (retained) austenite peak and {110} ferrite peak with the approximation of {111} austenite peak using the linear

background. This solution generate the higher ferrite (martensite) and lower (retained) austenite fraction (Figure 15).

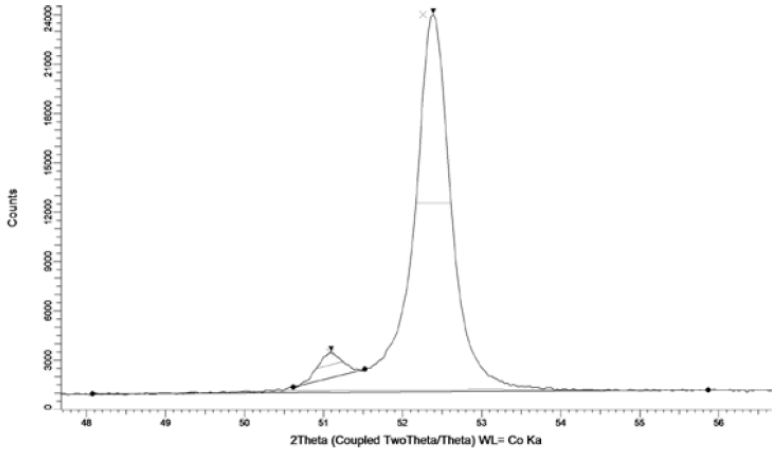

Figure 15 Schematic of the overlapping peaks on the X-Ray Diffraction curve [30]

The decomposition of retained austenite can be tracked by comparing the X-Ray Diffraction curve on the interrupted heating temperature with the un-reheated sample (Figure 16). It can be seen that generally the ferrite peaks on the reheating samples become sharper and slightly shifted indicating the increase of the ferrite-like phase (martensite, ferrite, or carbides).

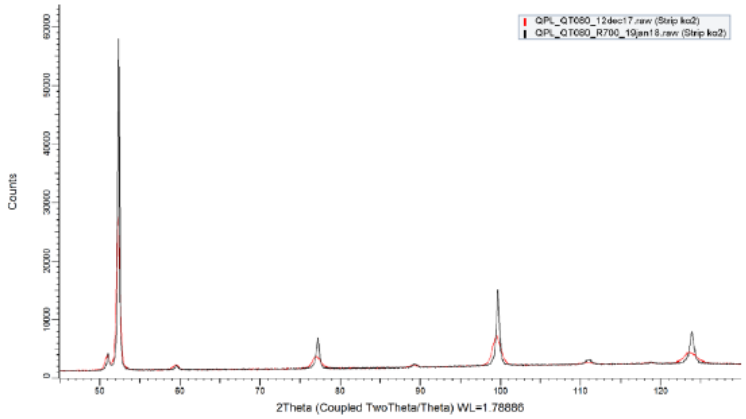

Figure 16 X-Ray Diffraction curve of the reheated and un-reheated samples. Colors are indicated on the graph

In order to count the carbon concentration in austenite, the following equation that relates the chemical composition of the alloy and lattice parameter of the respected phase is used [1]

$$\alpha_\gamma = 0.355\ nm + 0.0044\ \frac{nm}{wt.\%} X_c^\gamma \quad (2.13)$$

Where α_γ is experimental lattice parameter of austenite (explained in sub-section 2.4.2), whereas X_c^γ is the concentration of carbon, manganese, and aluminium in austenite. The error is reported 0.05 w.t % C [1].

2.4.2 Lattice parameter calculation: Nilsen-Riley method [32]

The lattice parameter is calculated from the same data acquired for calculating fraction of retained austenite. All obtained intensities are corrected with a fixed slit measurement (assuming 1° divergence and an irradiated length of 7 mm) after removal of the Co-Kα2 intensity using Bruker-Eva software. The diffraction peaks are later fitted with a pseiudo-voigt function using a least squares fitting algorithm. After being corrected, the lattice parameter can be estimated using Bragg`s law

$$\lambda = 2dsin\theta \quad (2.14)$$

where λ is the wavelength x-ray source, θ is the diffraction angle of the beam, and d is the interplanar distance that has following relation:

$$a = d\sqrt{h^2 + k^2 + l^2} \quad (2.15)$$

where a is the lattice parameter of the phase and (hkl) are correspond to the Miller indices of the reflecting plane. The calculated lattice parameter of the different peaks show deviation one another due to, as described above, the difference of the receiving and reflected intensities that is higher at higher θ. Therefore, the related error factor is calculated and the lattice parameter are presented as a function of θ:

$$a = a_0 + m\left[\frac{cos^2\theta}{sin\theta} + \frac{cos^2\theta}{\theta}\right] \quad (2.16)$$

where a_0 is the mean or representative lattice parameter, m is the slope, $\left[\frac{cos^2\theta}{sin\theta} + \frac{cos^2\theta}{\theta}\right]$ is the Nelson-Riley function. Figure 17 shows the lattice parameter as a function of Nelson-Riley value. The equation on the Figure 17 represented eq. 2.16. The value of a_0 is the intercept of the y-axis when Nelson-Riley value equal to zero ($\theta = 90$).

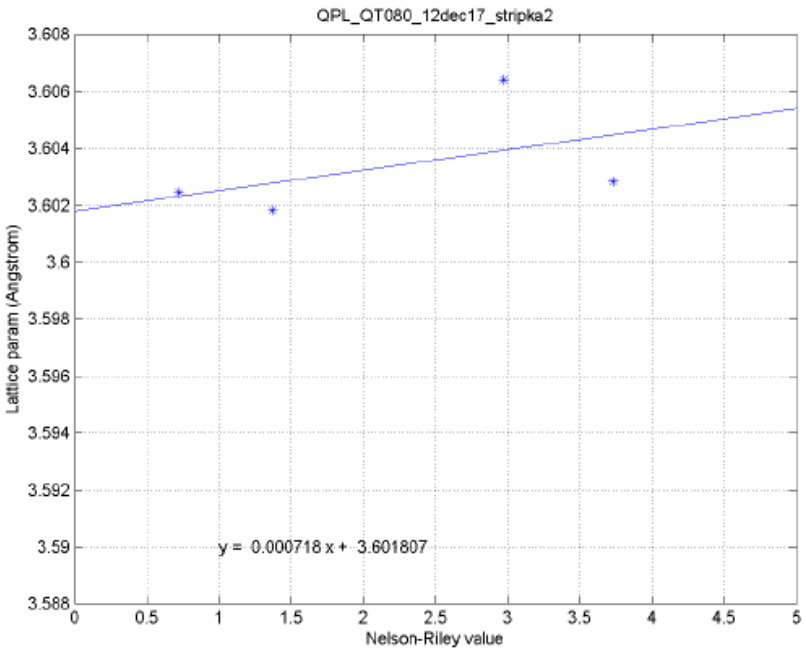

Figure 17 Example of lattice parameter calculation using Nilsen-Riley method [32]

2.5 Optical and scanning electron microscope

Since the resolution of the optical microscope is limited, fine features of the microstructure such as martensite or carbide cannot be captured well. Therefore, optical microscope is used only to give the overview of the microstructure and validated it with the literature. Furthermore, it is used to make sure that the sample is ready to put into scanning electron microscope (SEM) machine by means of the cleanliness and scratch free surface sample. Magnification up to 10X is used typically. In order to capture the fine features, SEM is used. In this research, all SEM pictures are taken at 2000X and 10.000X magnification.

A Keyence VHX-5000 series digital microscope is used to take the optical microscopy image, while a JEOL JSM-6500F series field emission gun SEM is operated using secondary electron imaging with 15 kV of acceleration voltage and 10 mm of working distance.

2.6 Hardness test

The Microhardness test is used in order to validate the observed phase after applying certain reheating process to the samples. In current work, vickers HV0.05 (0.05 kgf) is chosen since the indentation is not exceed the interest phase area. The average values of the hardness value is taken from five measurements in each samples where every indentation separated by five times of diagonal indentor.

Chapter 3: Results and Discussion

The chapter is divided into two sections, namely: microstructure of Q&P samples and study of the reheating process on Q&P samples.

3.1 Microstructures of Q&P samples

3.1.1 The critical temperatures

A_1 and A_3 temperatures describe the intercritical region in the equilibrium phase diagram. The A_1 temperature is defined as temperature at which eutectoid reaction ($\gamma \rightarrow \alpha + Fe_3C$) is observed, whereas the A_3 temperature relates to phase transformation of α-iron into γ-iron [29]. The equilibrium phase diagram of the Q&P steel can be constructed using ThermoCalc software (2017 version). From Figure 18, it is observed that the A_1 and A_3 are approximately 710 °C and 760°C. Even though all heat treatments conducted throughout this research are not in the equilibrium condition, knowing the equilibrium phase diagram will help the reader to understand the microstructural events at high reheating temperature.

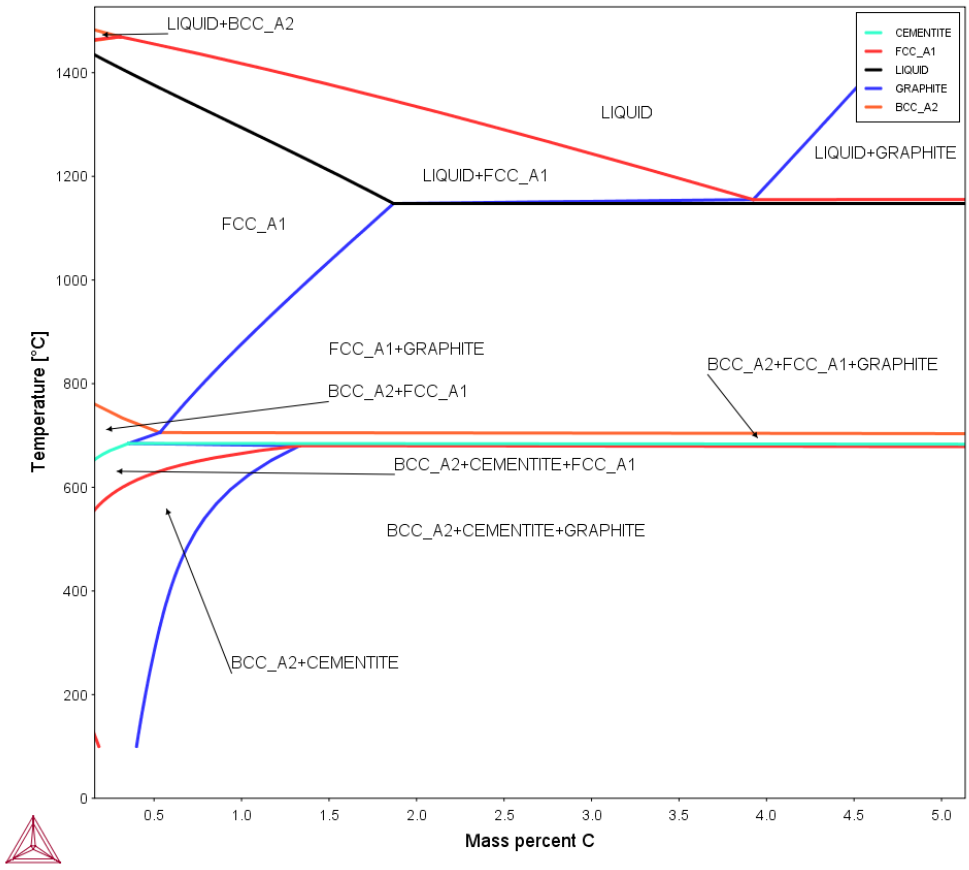

Figure 18 Equilibrium phase diagram of Q&P steel. Correspond phases are indicated on the figures. BCC_A2 is austenite, and FCC_A1 is ferrite.

The dilatometry curve is often used to determine the critical temperatures of the steels such as the M_s, Ac_1 and Ac_3 temperatures. M_s is observed by the change of the linearity of the dilatometry curve during quenching. It cannot be found in the phase diagram since the martensite is the product of an athermal phase transformation requiring rapid cooling. Ac_1 and Ac_3 (c stands for *chauffage* in French meaning heating) are above A_1 and A_3 since the selected heating rate is faster than the one which used to acquire the equilibrium condition. It means that Ac_1 and Ac_3 temperatures are heating rate dependent. The faster heating rate, the higher the A_c point [33].

The Ac_1 and Ac_3 temperatures are visible on the dilatometry curve by detecting the deviation of the linear thermal expansion or contraction during heating. In Figure 19, the Q&P steel is heated up to 1200°C with 2°C/s of heating rate. The critical temperatures can be observed approximately at 718°C and 820°C for Ac_1, and Ac_3, respectively. The full austenite condition can be observed by a linear increase of the thermal expansion upon the Ac_3 temperature, which is used later to determine the austenitization temperature.

A slight deviation of the linear thermal expansion is spotted at 467-518°C. It does not correspond to equilibrium phase diagram because there are no microstructural events within this temperature range. This change in length may be related to carbides precipitation.

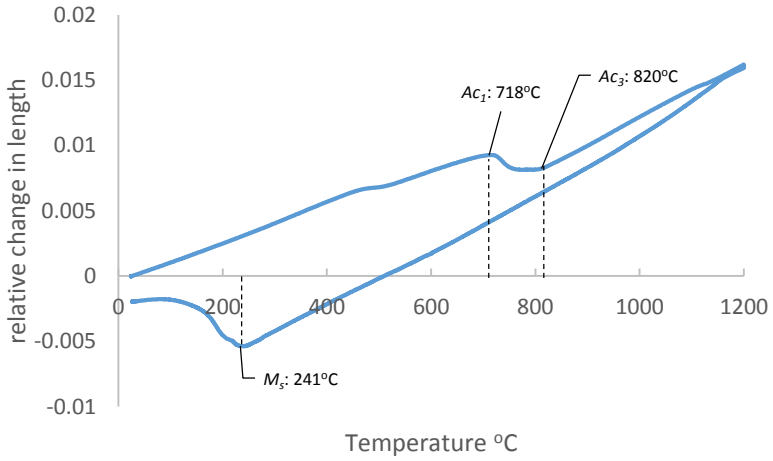

Figure 19 Dilatometry curve of the heated QP steel up to 1200°C. The observed critical temperature are indicated on the figure.

Martensite start (M_s) temperature is defined as the temperature below which the martensite phase start to form. Between other methods, the M_s temperature can be calculated using Bhadeshia [34] or van Bohemen [35] approaches. However, the manganese content of the Q&P steel exceeds the manganese limit fraction of both methods. Therefore, it is more convenient to use the experimental M_s (241°C) which is observed in the dilatometry curve of Q&P steel after quenching (Figure 19).

The fraction of martensite can be calculated using the Koistinen-Marburger KM equation (eq. 3.1):

$$f_{M1} = 1 - \exp[-\alpha(T_{km} - T)] \qquad (3.1)$$

where $f_{M1}$is martensite fraction, α is rate parameter, T_{km} is the theoretical martensite temperature, and T is the interest temperature. The martensite fraction (f_{M1}) can be fitted with the lever rule calculation of the dilatometry curve (Figure 20). A discrepancy is observed between the martensite fraction calculated by KM-equation and lever rule near the M_s temperature. It can be explained by the fact that the M_s temperature depends on its prior austenite grain size. The M_s temperature decreases as the prior austenite grain size becomes finer. It means that the discrepancy between M_s temperature and the T_{km} is less in the finer prior austenite grain size [36]. It is reported that the difference between both values are typically between 5-20ºC [35]

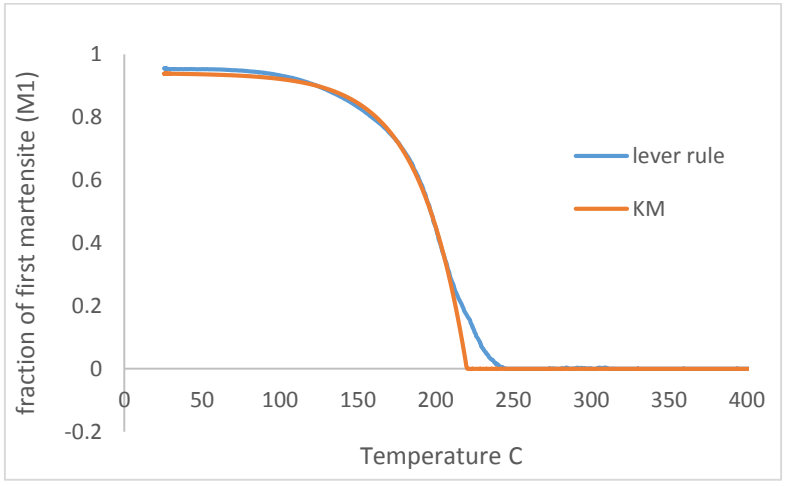

Figure 20 Martensite fraction evolution calculated by lever rule and KM-equation

In order to obtain the optimum fitted parameter (T_{km} and α), the solver function in Excel is executed by also using martensite and austenite fraction calculated by lever rule. The obtained values of T_{km} and α are 220ºC and 0.0327 K^{-1}. These values are used to determine the fraction of martensite faced at every quenching temperature later.

3.1.2 Q&P heat treatment

The Q&P steel samples are heat treated in the dilatometer as explained in section 2.2. The applied austenitization temperature is 900ºC, whereas the austenitization time is selected to be 180 s based on the assumption that at the selected temperature the parent phase already transformed entirely into austenite and as further austenitization process continues, there is enough time to let the carbon homogenized throughout the sample. Thus, the whole samples are austenized at 900ºC and held for 3 minutes in order to achieve the full austenite condition.

After the austenitization process is done, the sample is quenched to various quenching temperatures between the M_s and M_f temperatures in order to generate different combinations of the martensite and austenite fractions in the microstructure. In this experiment, various quenching temperatures are chosen in the temperature change of 80-280ºC. In addition, a cooling rate of 40ºC/s is chosen. This cooling rate avoids the nose curve associated with ferrite, bainite, and pearlite. In Figure 21 (a), it can be seen that as the alloying element increases, the nose curve is shifted to the right. It implicates that a wider range of cooling rates can be applied in order to form martensite. The time temperature transformation (TTT) diagram (Figure 21.b) corresponds to the current Q&P steel composition and is constructed using Bhadeshia's model [34]. It shows that the selected heating rate implies the formation of martensite without crossing the bainitic region. A very short holding (3 s) at the quenching temperature is chosen to avoid the formation of bainite and carbides. The process is continued with the partitioning step.

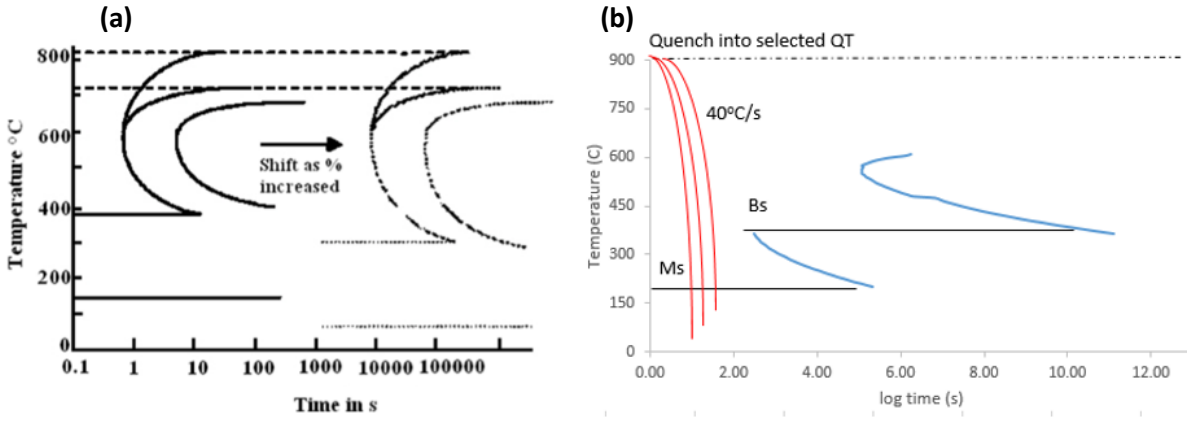

Figure 21 (a) influence of the alloying element on nose curve in TTT diagram [37]. The figure show that the nose curve is shifted to the right as the fraction of alloying elements increase. (b) The TTT diagram of the current Q&P steel calculated using Bhadeshia calculation [27]

The partitioning process is applied at 400ºC for 50 s to let all the carbon atoms diffuse from the martensite to austenite. The partitioning temperature of 400ºC is chosen since it is higher than the M_s temperature so new martensite will not be formed during the partitioning step [24].

Finally, the process ends by quenching the samples to room temperature with the same cooling rate as the first quenching process (40ºC/s). The applied Q&P heat treatments can be seen in Figure 22.

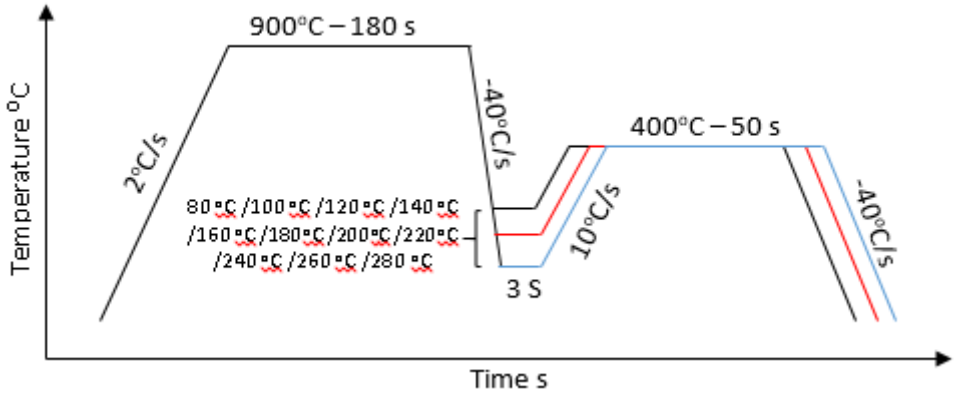

Figure 22 The Q&P treatments. All related parameters are indicated on the graph

3.1.3 Phases fractions

The final microstructures after the application of the heat treatments in Figure 22 consist of tempered martensite (f_{M1}), retained austenite (f_{RA}), untempered martensite (f_{M2}), and possibly bainite (f_B), even though the latter phase is theoretically suppressed by introducing manganese as alloying element. The summation of the fractions of all these phases is unity.

$$f_{M1} + f_{RA} + f_{M2} + f_B = 1 \qquad (3.2)$$

M_1 corresponds to martensite formed at the first quenching that is tempered at the partitioning temperature (400°C in this case) during the partitioning step. The formation of M_1 is characterized by the deviation of the linear thermal contraction in the dilatometry curve during the first quenching. Figure 23 shows dilatometry curves during cooling to quenching temperature of two samples (QP80 and QP160) as examples to illustrate the linear contraction up to the M_s temperature followed by an expansion indicating the formation of M_1.

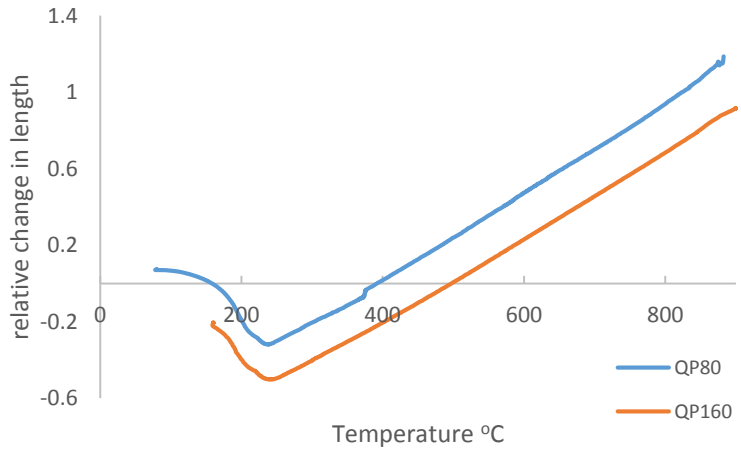

Figure 23 Typical dilatometry curve during first quenching. The legend is indicated in the picture

The f_{M1} is calculated with the KM-equation using the optimum fitted parameter mentioned in section 3.1.1. Figure 24 shows f_{M1} as a function of the applied quenching temperatures to the different samples.

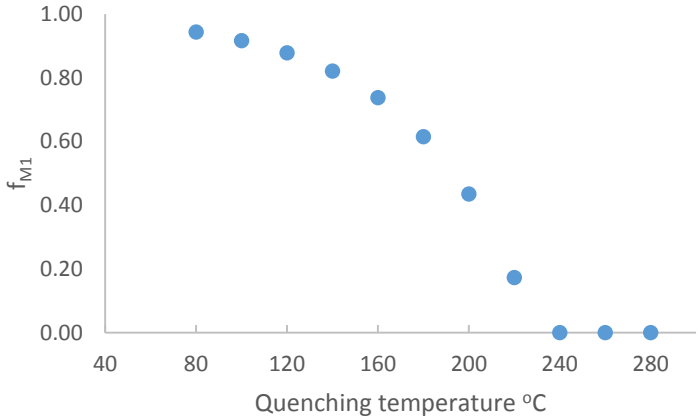

Figure 24 f_{M1} calculated by KM-equation using the optimum fitted parameters

It can be seen in Figure 24 that the f_{M1} of the 240 °C, 260 °C, and 280°C quenching temperatures are assumed to be zero and cannot be predicted using KM equation since that quenching temperature are above the calculated KM martensite start temperature, T_{km} (230°C). The remaining values show that the f_{M1} increased as the sample quenched into lower quenching temperature with 0.943 of f_{M1} at 80°C of quenching temperature. The formation of a higher fraction of martensite fraction implies more carbon available for partitioning to austenite in the partitioning step.

On the other hand, the volume fractions of retained austenite, $f_{RA,}$ are obtained from X-Ray Diffraction measurements (Figure 25) and using the Jatczak method (section 2.4.1). The f_{RA} shows a bell-like curve. There is a maximum f_{RA} (18.3 ± 0.3 %) at 160°C, which gradually decreases in either direction with respect to 160°C of quenching temperature.

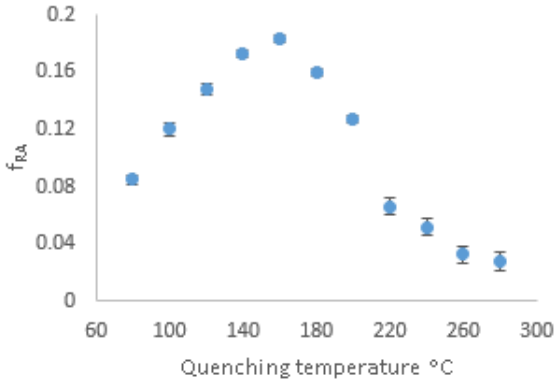

Figure 25 f_{RA} as a function of quenching temperature

Figure 26 (a) shows the lattice parameter and carbon content in retained austenite with respect to the quenching temperature. The lattice parameter of retained austenite is slightly affected by the quenching temperature. A slight increase is observed to start from quenching temperature 140ºC to 80ºC showing that more f_{M1} means higher carbon content in the austenite (higher lattice parameter). At the quenching temperature of 220ºC and 240 ºC, an apparent decrease of the lattice parameter is observed.

Figure 26 (b) shows the relation between the carbon content in retained austenite and f_{RA}. It can be seen that the carbon content in austenite increases as the f_{RA} increases up to 1.18 w.t % of carbon content in austenite above which it shows a relatively constant value regardless of the respected $f_{RA.}$

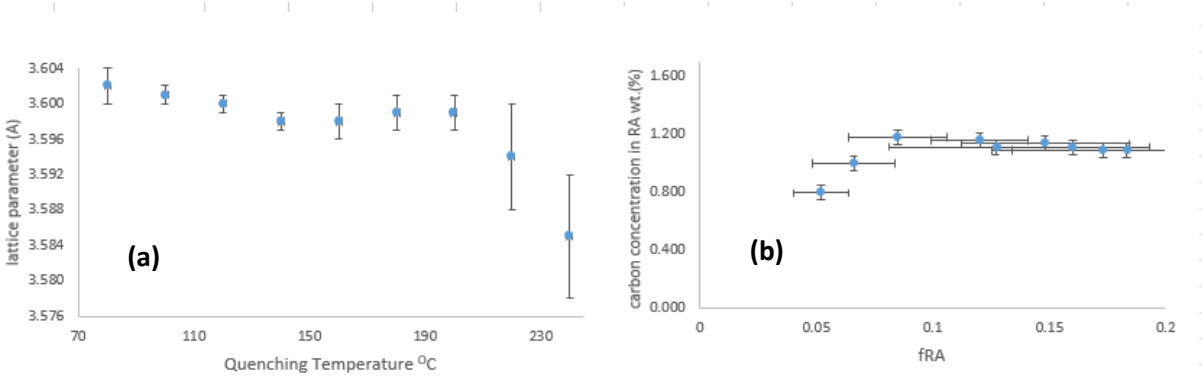

Figure 26 (a) lattice parameter and (b) carbon concentration in retained austenite with respect to quenching temperature

Although competing reactions during the partitioning step were expected to be suppressed by the presence of manganese, it seems that bainite forms. This can be observed in Figure 27 by an expansion in the dilatometry curve during the partitioning process. The largest expansion observed was of approximately 0.1 % at 180ºC and 200 ºC of quenching temperature. These expansions correspond to 0.17 and 0.10 of f_B as calculated from eq. 2.9. In general, the observed expansions decrease as the quenching temperature decreases because the bainite formation can be avoided at lower quenching temperatures as it moves further away the bainite start temperature. Moreover, less austenite availability at lower quenching temperature specimen makes the bainite transformation unlikely to occur. Contraction observed at 220 ºC and 240 ºC of quenching temperature during the partitioning step might be correlated with austenite growth or carbide precipitation.

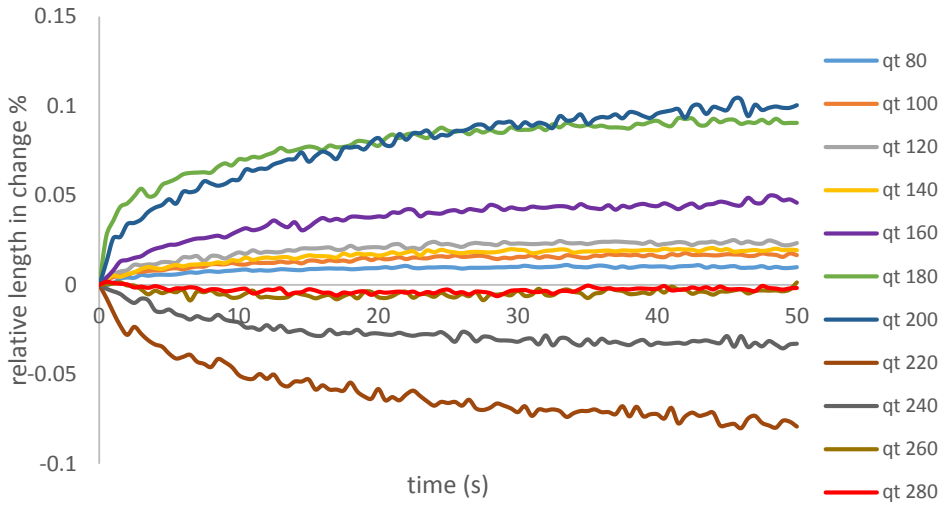

Figure 27 The relative length change during partitioning process. The legend is indicated on the graph

Finally, the f_{M2} can be obtained by balancing eq. 3.2. Similar with the M_1, the formation of M_2 can be observed in the corresponding dilatometry curve during the second quenching after the partitioning step. In Figure 28, the expansion during cooling to room temperature observed in specimen QP240 indicates the formation of M_2, whereas no M_2 formation is observed in specimen QP80.

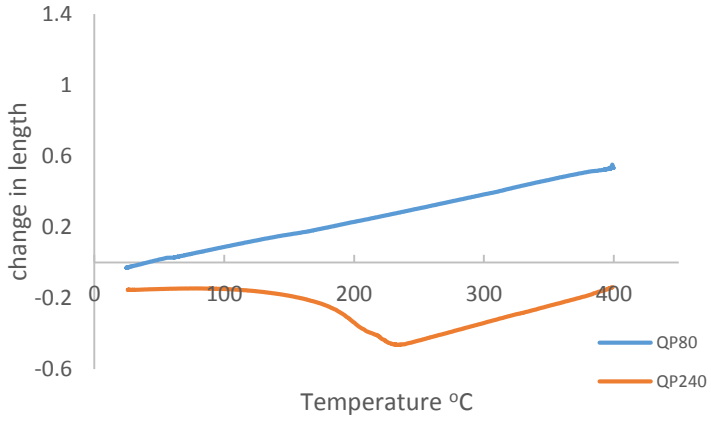

Figure 28 typical dilatometry curve during second quenching. The legend is indicated on the figure

The complete comparison of the constituents phase fraction can be seen in Figure 29. It can be seen that bainite is suppressed below the optimum quenching temperature of 160°C above which its fraction start to grow up to 200°C of quenching temperature. M_2 is also suppressed below quenching temperature of 160°C and then it increases with quenching temperature. f_{M1} decrease as increasing quenching temperature because the quenching temperature is approaching M_s temperature.

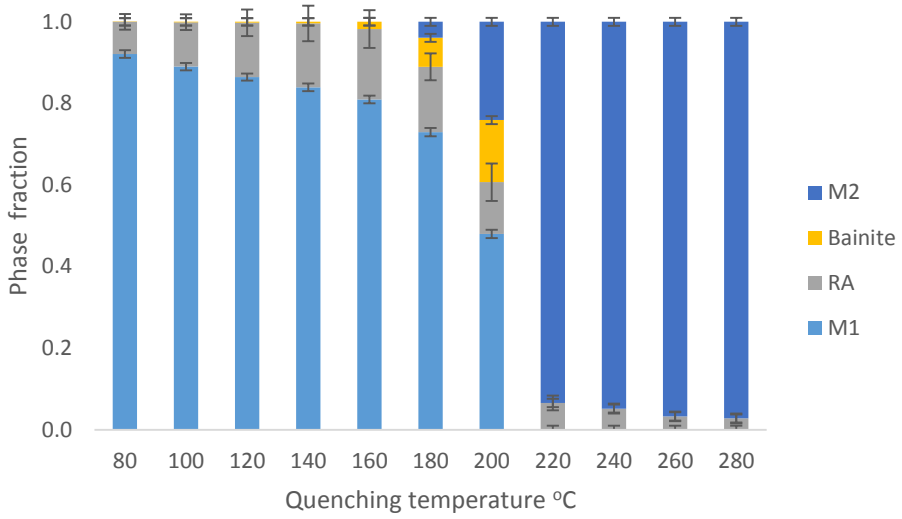

Figure 29 Phase fraction of all constituents as a function of quenching temperature

3.1.4 Microstructures of the QP samples

The SEM pictures of samples QP80 and QP160 are selected to be presented here because of their representativeness. Figure 30 shows the microstructure of the specimen QP80 at two different magnifications. It displays a typical Q&P microstructure characterized by ellipsoid carbides which are dispersed within the M_1 matrix (dark region) and retained austenite (light region) either in film or blocky type surrounded by the M_1.

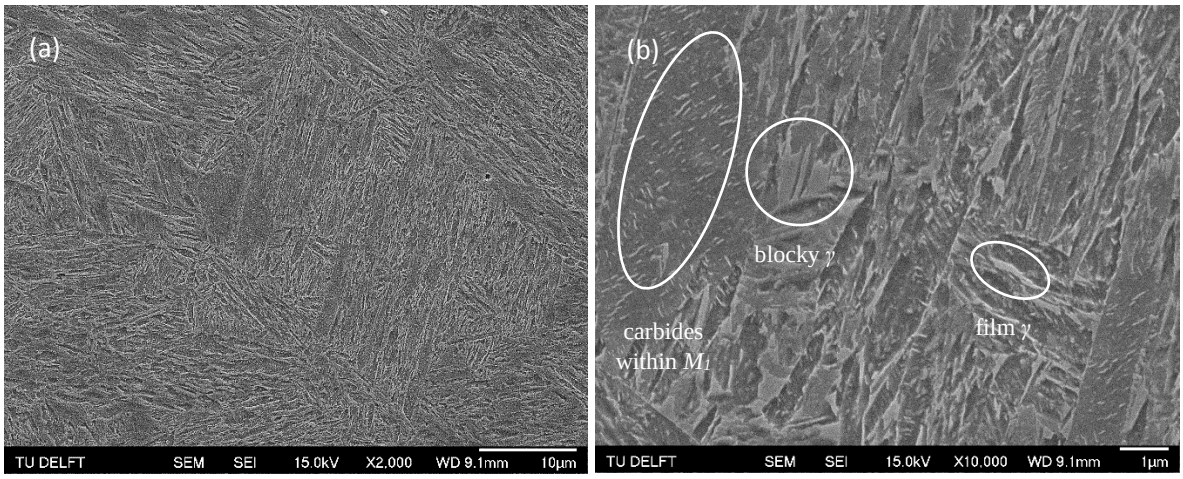

Figure 30 SEM pictures of QP80. (a) 2000X and (b) 10.000X magnification

Similar to QP80, the QP160 microstructure (Figure 31) also consists of a combination between lath martensite (dark region) and retained austenite (light region). Interestingly, the ellipsoid carbides features are not only present within the M_1 matrix but also at the tip of the retained austenite phases.

Another feature observed is Martensite-Austenite (MA) islands. Indicating two phases present there, namely un-tempered martensite (M_2) surrounded by retained austenite (light region).

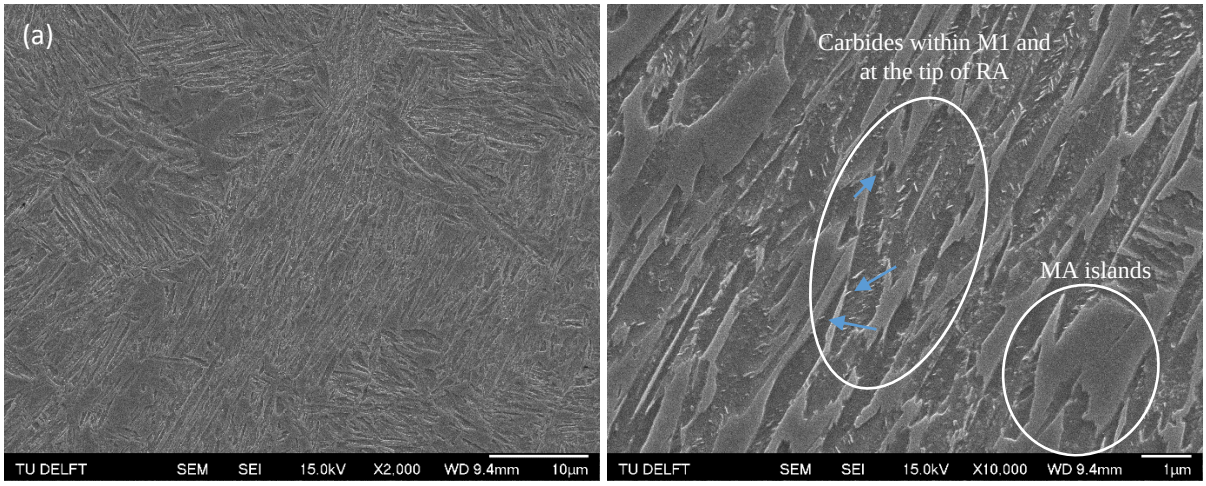

Figure 31 SEM pictures of QP160. (a) 2000X and (b) 10.000X magnification. Blue arrows shows the carbides at the tip of retained austenite

3.2 Study of reheating process on Q&P samples

3.2.1 Reheating up to 700°C

To study the thermal stability of the retained austenite, the Q&P samples are reheated to 700°C and quenched to room temperature subsequently. The reheating temperature is chosen because it lies below the A_1 temperature on the equilibrium phase diagram avoiding the formation new austenite (Figure 18). The heating rate of 5°C/s is chosen with the assumption that the heating rate is slow enough to allow the carbon diffusion to happen. Finally, the reheated samples are directly quenched with the high rate of cooling (-200°C/s) in order to capture the high-temperature microstructure. All parameters of the reheating process are indicated in Figure 32.

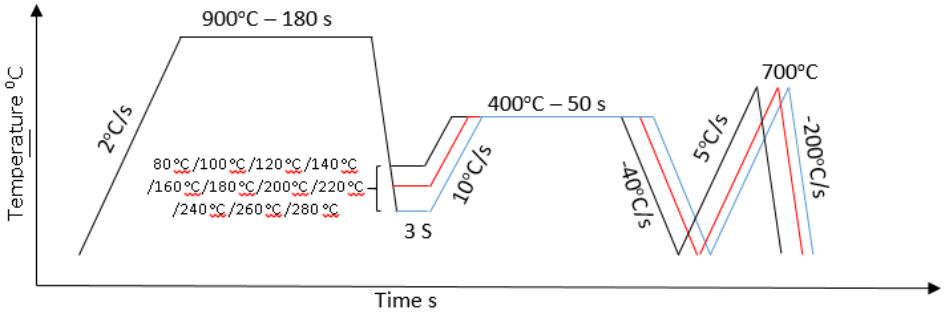

Figure 32 Reheating process up to 700°C on Q&P samples. All parameters are indicated on the figure

Figure 33 shows the comparison of f_{RA} with respect to the quenching temperature between the un-reheated and reheated samples. The f_{RA} after reheating shows a different trend than the samples subjected only to Q&P treatments. The f_{RA} loses its dependency on quenching temperature and lies on the relatively same fraction values regardless of the quenching temperature, namely in the range of 0.05-0.08 (Figure 33). Most of the samples are showing the decreasing amount of f_{RA} (green arrow in Figure 33), whereas the increasing amount of f_{RA} is also found at the high quenching temperature (black arrow in Figure 33). In order to obtain more insight on this phenomenon, the highest drop of f_{RA} (QT160°C) and the lowest drop of f_{RA} (QT 80°C) are further studied by reheating up to 900°C as well as by performing interrupted reheating treatments to lower temperatures followed by quenching to room temperature.

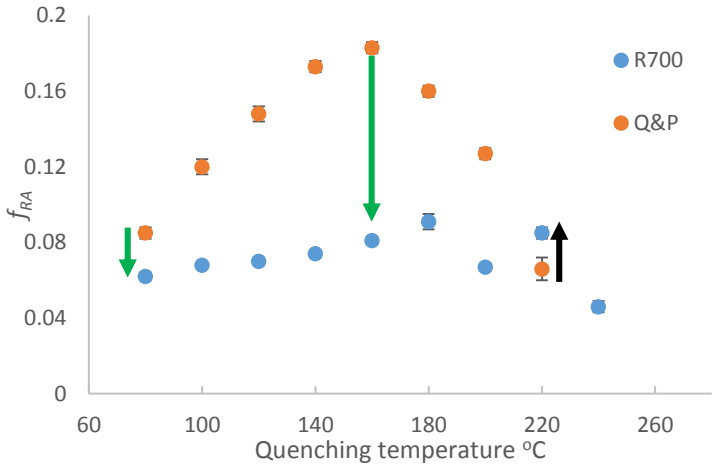

Figure 33 Before and after reheating comparison of f_{RA}. R700 means reheating up to 700°C. Green arrows indicated the largest and lowest decrease of f_{RA}

3.2.2 Reheating up to 900°C

Specimens QP80 and QP160 are reheated up to 900°C (Figure 34) in order to study the microstructural events occurring at elevated temperatures. As discussed, two quenching temperature are chosen since they have lowest and highest drop of the f_{RA} after reheating up to 700°C. On the other hand, the extended reheating temperature (900°C) is chosen to cross the fully austenitic region. The heating and cooling rates are chosen for the reasons indicated in section 3.2.1. The samples will be analyzed by means of dilatometry curve, X-Ray Diffraction, and relevant microstructures.

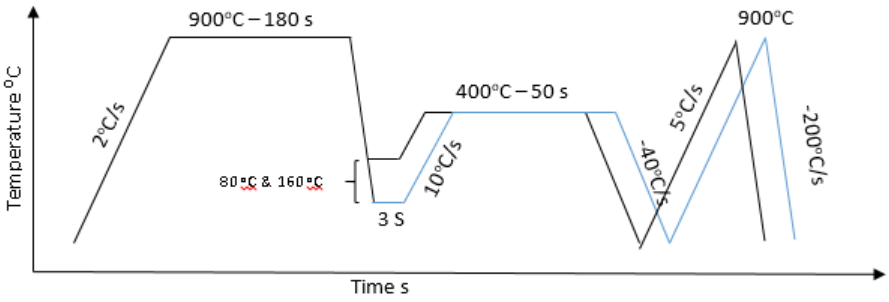

Figure 34 Reheating process up to 900°C on selected Q&P samples. All parameters are indicated on the figure

3.2.2.1 Reheating of QP80

Figure 35 shows the dilatometry curve (a) and its respected derivative curve (b) of the QP80 during reheating up to 900°C. Six changes in slope are observed at around 470°C, 530°C, 700 °C, 720 °C, 750°C, and 790°C. These might be related to the decomposition of the retained austenite, carbides precipitation, and new austenite formation as well as the end of these phenomena

A slight contraction corresponding to carbides precipitation is observed around 470°C, ended at around 530°C. It seems that cementite formed and replaced the transitional carbide in this temperature range since this relative changes in slope is observed at relatively high reheating temperature [38]. The remaining changes in slope are related to the austenitization process characterized by an unusual anomaly at the onset of the austenitization process (around 700°C) similar found in [39]. It seems that the austenitization takes place in three consecutive steps, namely: carbide dissolution (which corresponds with an expansion between 700°C and 720°C), (martensite and) carbide to austenite transformation (which corresponds with a contraction between 720°C and 750°C), and further formation of austenite from the tempered martensite matrix until the microstructure becomes fully austenitic (which corresponds with a contraction between 750°C and 790°C).

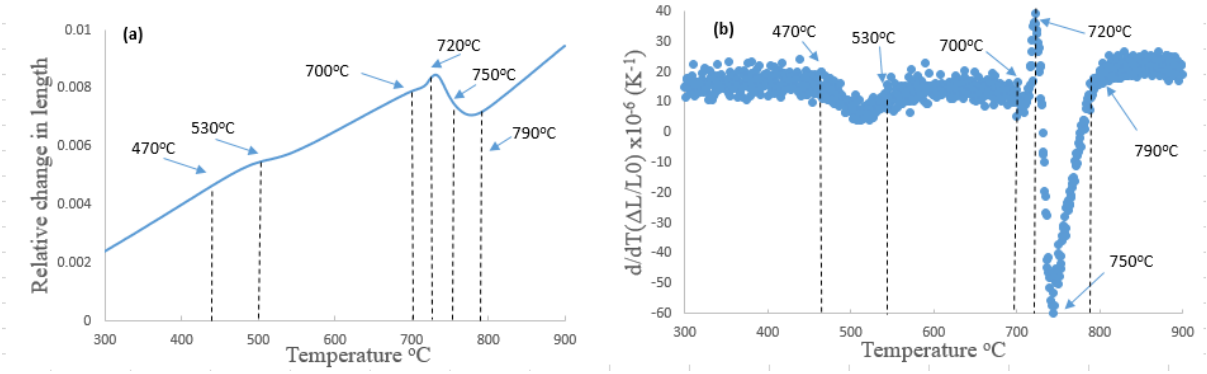

Figure 35 (a) dilatometry curve and (b) its derivative of heated QT80 up to 900oC. The observed changes in slope are indicated on the graph

Further interrupted reheating is applied at lower temperatures to check the proposed microstructural changes. The samples are reheated up to 450ºC, 530ºC, 610ºC, 720ºC, and 740ºC and directly quenched. Figure 36 shows the comparison of the cooling curve between all interrupted reheating samples. It can be seen that martensite formation (red arrow in Figure 36) is found at QP80R740 but not in the rest of the samples. This confirms the formation of austenite after reheating up to 740ºC.

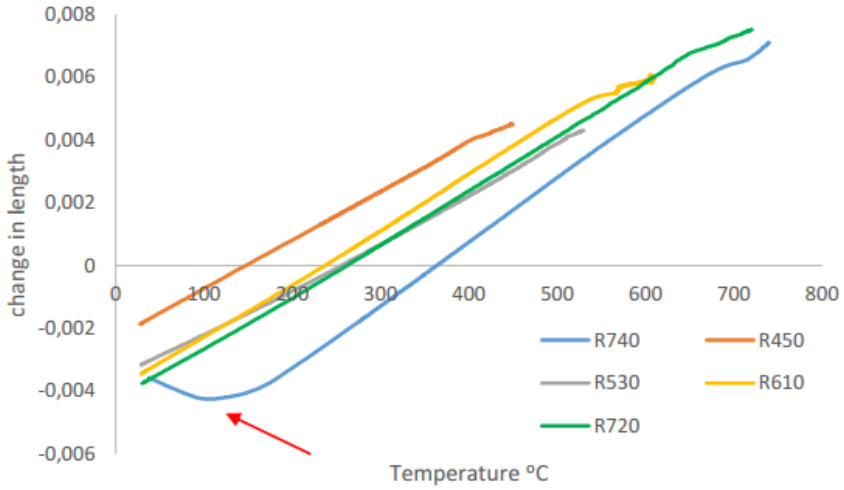

Figure 36 Dilatometry cooling curve of reheated QP80. The reheating temperature of each sample is indicated with colours. Red arrow indicates the martensite formation upon quenching after reheating. It is only observed on QPR740 (blue line)

The SEM pictures of all interrupted reheating of QP80 samples upon quenching are analyzed. The samples are interrupted at 450, 530, 610, 720, and 740ºC of reheating temperature.

- Microstructure after reheating to 450ºC

Figure 37 shows SEM pictures of QP80R450 sample. In Figure 37(b), ellipsoid carbides are observed within M_1 matrix. Furthermore, there are also situated next to each other as a discrete particles in certain length similar to film type of retained austenite. The film and blocky type of retained austenite are also seen. The obtained microstructures are similar to the QP80 microstructure explaining no significant microstructural events took place yet upon reheating to 450ºC.

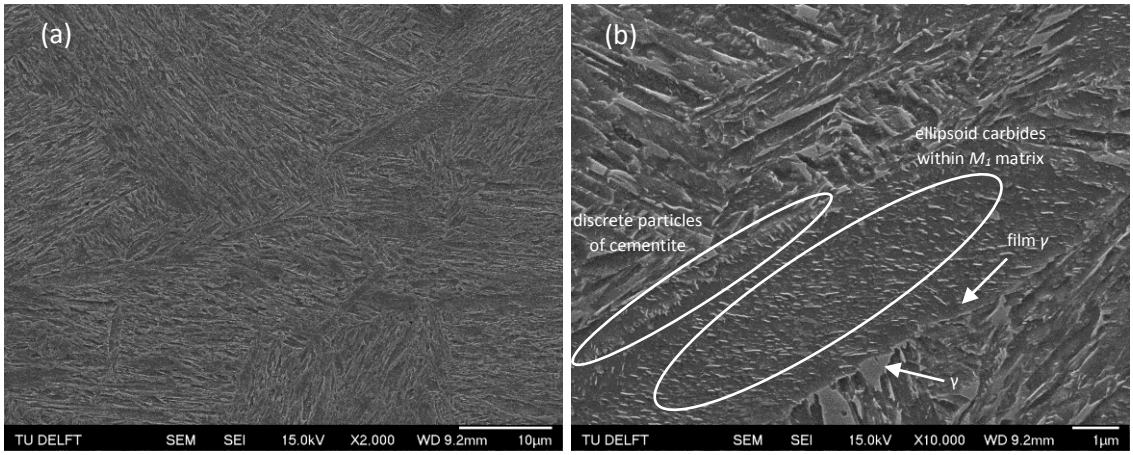

Figure 37 SEM pictures of QP80R450. (a) at 2000X magnification and (b) at 10.000X magnification. The white circles and arrows indicated the observed features on the microstructures

- Microstructure after reheating to 530ºC

Figure 38 shows SEM pictures of QP80R530 sample. In Figure 38(b), ellipsoid carbides within M_1, discrete particles of cementite, globular carbides, and film type austenite are observed. It can be seen that after reheating to 530ºC, two types of carbides are identified, namely: ellipsoid and globular carbides. The ellipsoid carbides are dominant over the globular ones. However, the obtained microstructures are still similar to the QP80 sample. It is difficult to reveal the reason for the relative changes in slope between 470ºC and 530ºC.

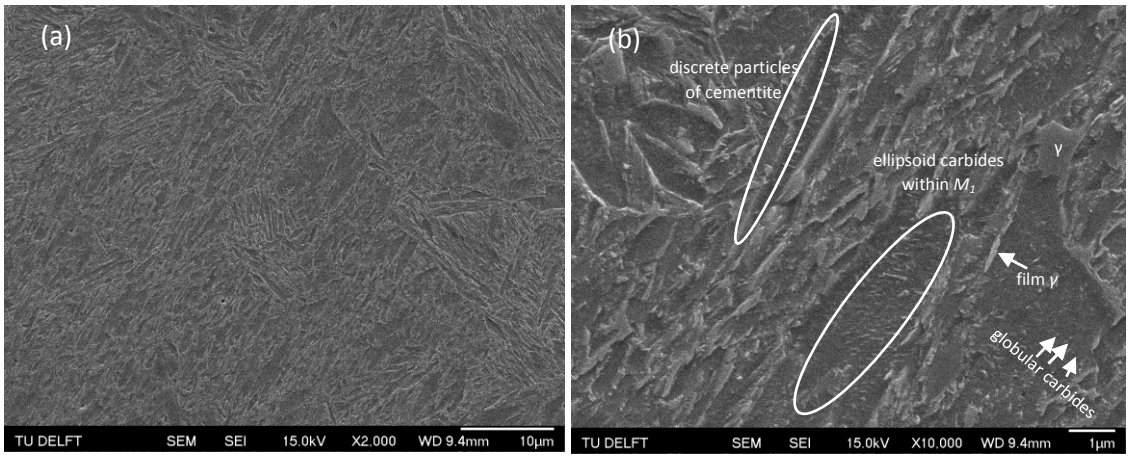

Figure 38 SEM pictures of QP80R530. (a) at 2000X magnification and (b) at 10.000X magnification. The white circles and arrows indicated the observed features on the microstructures

- Microstructure after reheating to 610ºC

Figure 39 shows SEM pictures of QP80R610 sample. In Figure 39(b), it can be seen that less ellipsoid carbides are observed within M_1 matrix. Discrete particles of cementite are also seen near the M_1 matrix. On the other hand, globular carbides are observed more than ellipsoid carbides within the M_1 matrix.

The discrete particles of cementite are also spotted near M_1. Film type and blocky type of austenite are also spotted in Figure 39(b). Hence, the relative changes in slope at 470°C and 530°C are related to more carbide precipitation. In particular, the formation of globular carbides.

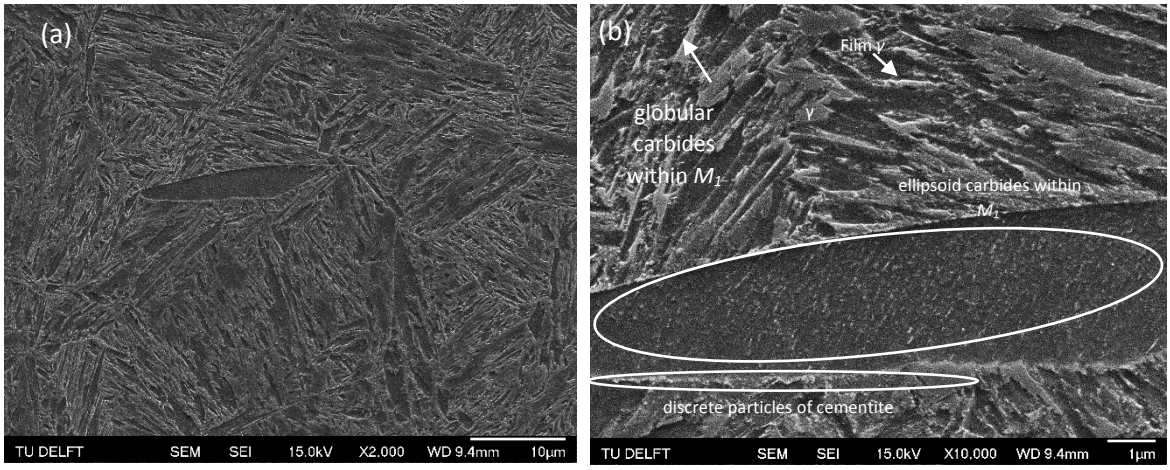

Figure 39 SEM pictures of QP80R610. (a) at 2000X magnification and (b) at 10.000X magnification. The white circles and arrows indicated the observed features on the microstructures

In summary, the observed features comparison in the microstructures of QP80R450, QP80R530, and QP80R610 samples can be found in Table 3.

The film and blocky type austenite present in all three samples indicate that these features remain after reheating up to 610°C. Nevertheless, it seems that some film type austenite decomposes into discrete particles of cementite which can be observed in all three samples. It is also observed that ellipsoid carbides within M_1 matrix are present predominantly in QP80R450. The globular carbides within M1 matrix start to be detected in QP80R530 and became more dominant compared to ellipsoid carbides in QP80610. It means that after reheating up to 610°C, some ellipsoid carbides seem to dissolve and are replaced by the new globular carbides.

Table 3 The observed features comparison in microstructures of QP80450, QP80530, and QP80610

Samples	Features
QP80R450	Ellipsoid carbides can be found within M_1 matrix
	Blocky type austenite
	Film type austenite. Some decompose into discrete particles of cementite
QP80R530	Ellipsoid carbides can be found within M_1 matrix
	Globular carbides start to be detected
	Blocky type austenite
	Film type austenite. Some decompose into discrete particles of cementite
QP80R610	Less ellipsoid carbides are observed comparing to QP80R450 and QP80R530.
	Globular carbides are more dominant than the ellipsoid carbides

	Blocky type austenite
	Film type austenite. Some decompose into discrete particles of cementite

- Microstructure after reheating to 720ºC

Figure 40 shows SEM pictures of QP80R720 sample. Globular carbides are seen throughout the micrograph. They can be observed in the M_1 matrix and grain boundaries of retained austenite. In contrast, ellipsoid carbides are hardly found anywhere. The obtained microstructures are similar to the ones observed in the microstructure of QP80R610 sample. Therefore, the slight contraction between 700ºC and 720ºC can be related to the dissolution of ellipsoid carbides and formation of globular carbides.

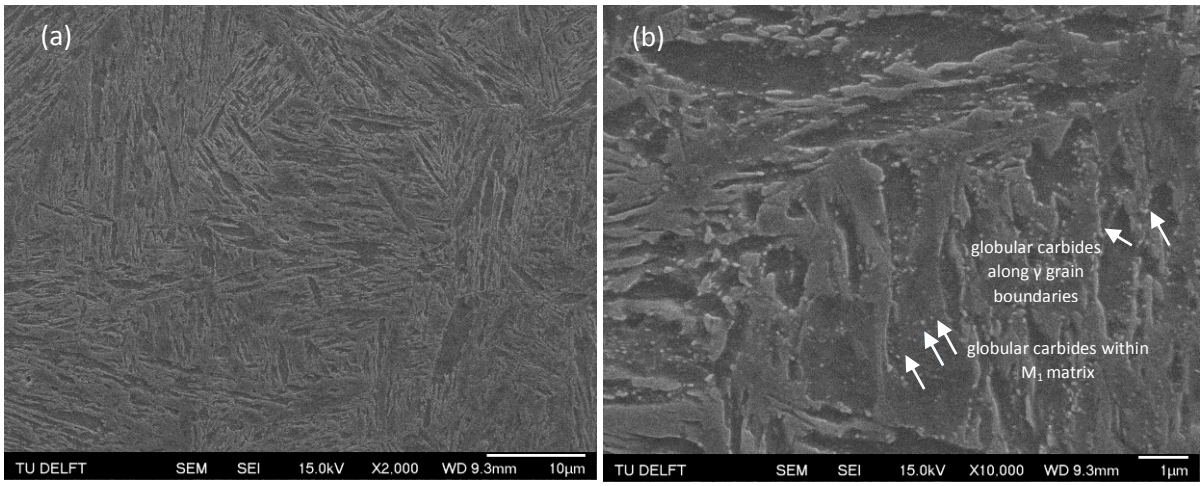

Figure 40 SEM pictures of QP80R720. (a) at 2000X magnification ; (b) and (c) at 10.000X magnification. The white arrows indicated the observed features on the microstructures

- Microstructure after reheating to 740ºC

Figure 41 shows the optical microscopy microstructure of QP80R740 sample. It consists of the river-like patterns (red arrows) that surrounded the suspected martensite (dark region). In Figure 41(b), it can be seen that the river-like features do not contain any inclusion or precipitates.

Micro-hardness tests (0.05 kgf) are performed in order to clarify the phase of river-like patterns by comparing its hardness with the dark region. It is obtained that the river-like pattern shows a hardness of 619.4 ± 6 HV. This is higher than the hardness of the dark regions which showed 544.8 ± 5 HV. This indicates that the river-like patters are formed by martensite that originally came from new austenite forming during reheating process. It can be said that the contraction between 720ºC and 750ºC is related to the formation of new austenite from (martensite and) carbide similar with [39].

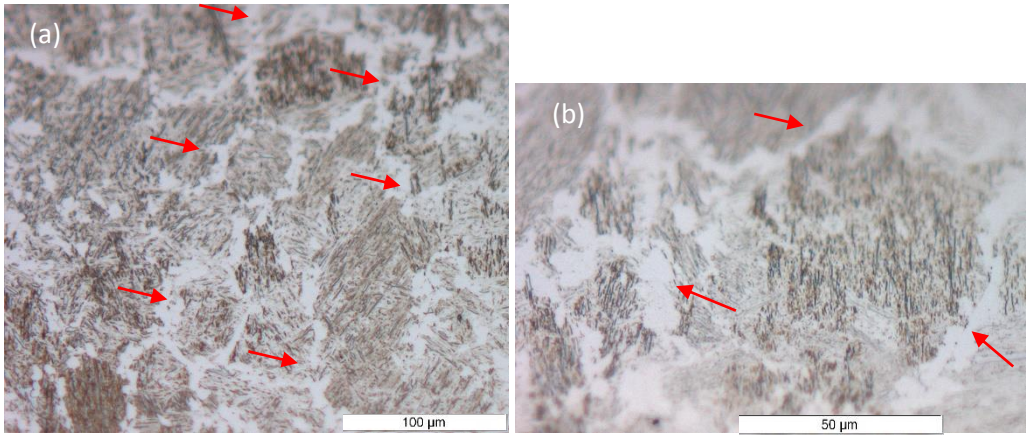

Figure 41 OM pictures of QP80R740. (a) at 5X magnification and (b) at 20X magnification. The red arrows indicated the river like pattern that surrounded martensite

The observed features after comparison between the microstructures of QP80R720 and QP80R740 can be found in Table 4.

Table 4 The observed features comparison in microstructures of QP80720 and QP80740

Samples	Observed features
QP80R720	Globular carbides can be found throughout the microstructures, namely within M_1 and austenite grain boundaries
QP80R740	River-like pattern relates to new austenite formation. It surrounded the dark region. It does not contain inclusion or precipitates

- X-Ray Diffraction curve of the interrupted reheating QP80 samples

X-Ray diffraction curves can be used to verify the discussion above. In the Figure 42, it can be seen that the intensity of the austenite peaks, namely {111}, {200}, {220}, and {311}, decrease after QP80 samples reheated up to 610^{o}C. It indicated the retained austenite decomposition phenomena which observed in Figure 37-40. On the other hand, the intensity of the austenite peaks in QP80R720 (green lines) and QP80R740 (purple line) increased indicating the new formation of austenite. Two overlapping ferrite peaks are observed in the QP80R740 (purple line in Figure 42). Those are overlapping with the normal ferrite peaks and makes the ferrite peaks to loss their symmetry. It can be

related to the martensite formation, which originally came from new austenite, upon quenching after reheating process as described in Figure 35.

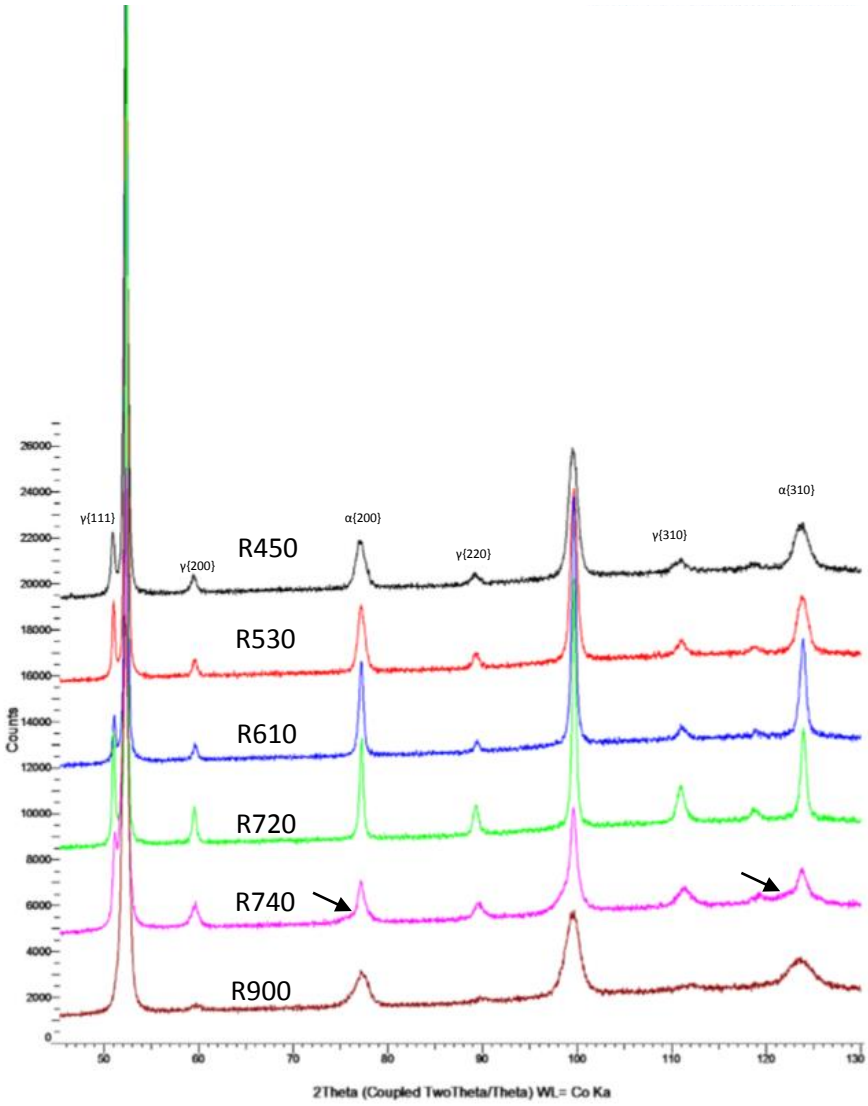

Figure 42 X-Ray Diffraction curve for QP80 after reheating up to 900oC. Colors explanation and ferrite & austenite peaks are indicated in the picture. Black arrows are indicated the overlapping ferrite peaks

- f_{RA} evolution during reheating process

The f_{RA} evolution during reheating process with respect to reheating temperature can be seen in Figure 43. It is observed that the f_{RA} dropped after reheating to 600°C. The f_{RA} increases again after reheated up to 720°C and higher since it entered the intercritical region and new austenite is expected to be formed.

Figure 43 can be used to confirm what is observed in the microstructure of all interrupted heating samples above. The decreasing value of f_{RA} after reheating up to 610°C (orange arrow) can be

described by retained austenite decomposition into ferrite and carbides as observed in QP80R610, whereas the increasing value of f_{RA} after reheating up to 720°C showed that the new austenite formation is observed. This is verified by the presence of additional ferrite peaks in QP80720 corresponding to martensite that originally comes from austenite (black arrows in Figure 42). It is formed upon quenching to the room temperature.

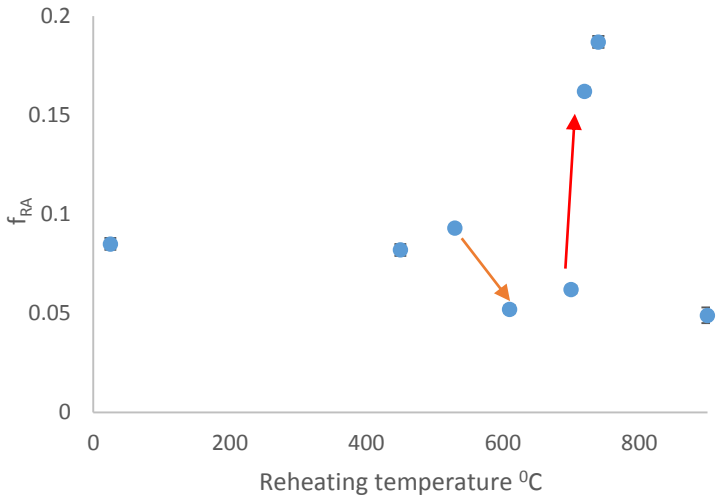

Figure 43 f_{RA} evolution of QP80 during reheating up to 900oC

- Summary: Reheating of QP80

Interrupted reheating processes are applied on QP80 samples. The formation of globular carbides within M_1 matrix and discrete particles of cementite from the film type austenite are observed after QP80 samples reheated up to 610°C. Those are correlated with the changes in slope observed between 470°C and 525°C in Figure 35. This explains the fact that retained austenite fraction decreased into constant value after reheating process.

The river-like structure surrounded the dark region are observed in QP80R740. From the hardness value comparison it can be said that the river-like patterns (light region) consisted mainly of martensite that originally came from the new austenite.

3.2.2.2 Reheating of QP160

Figure 44 shows the dilatometry curve (a) corresponding to reheated Q&P samples up to 900ºC and its respected derivative curve (b). Six changes in slope are observed, namely at 470ºC, 580 ºC, 690 ºC, 720 ºC, 745ºC, and 800ºC.

The carbide precipitation is expected to be observed at the reheating temperature range of 470ºC and 540ºC. It is characterized by a slight contraction at a relatively high reheating temperature [38]. The remaining changes in slope are situated very close to each other indicating the expected microstructural events which occurred consecutively, namely: carbide dissolution at 690ºC-720ºC, (martensite and) carbide to austenite transformation at 720ºC-745ºC, and further formation of austenite at 745ºC-800ºC.

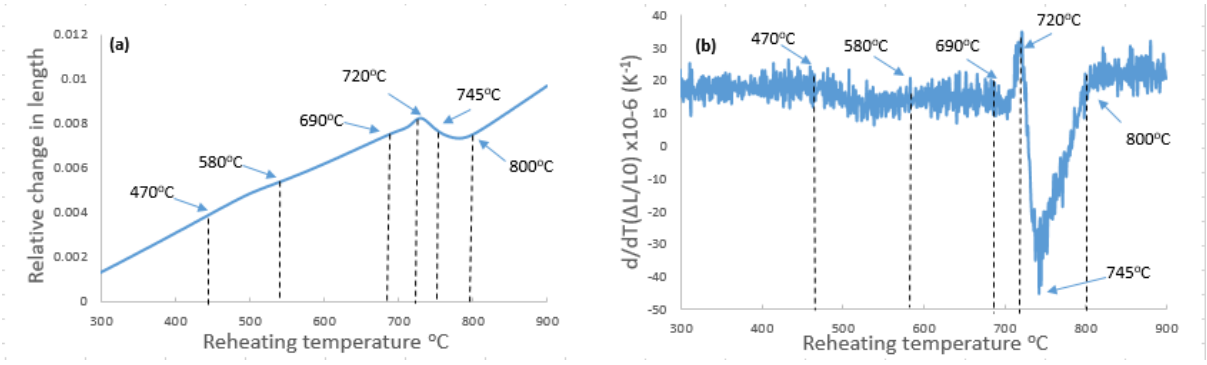

Figure 44 (a) dilatometry curve and (b) its derivative of the reheated QP160 up to 900oC. The observed changes in slope are indicated on the graph

Interrupted reheating at several temperatures, namely: 470ºC, 540 ºC, 690 ºC, 710 ºC, 720ºC, and 740ºC are applied in order to capture the mechanisms leading to the mentioned changes of slope upon reheating. Figure 45 shows the comparison of the cooling curve between all interrupted heating samples. It can be seen that martensite formed after reheating up to 610ºC, 720ºC, and 740ºC. After reheating to 610ºC, no new austenite formed since it did not cross the intercritical region. Therefore, the martensite can be formed from the unstable austenite after reheating. It means that after reheating at 610ºC (some) retained austenite is destabilized probably due to escape of the carbon to the martensite matrix and subsequently formed carbides. On the other hand, after reheating up to 720ºC and 740ºC new austenite formed and transformed into martensite upon quenching to room temperature.

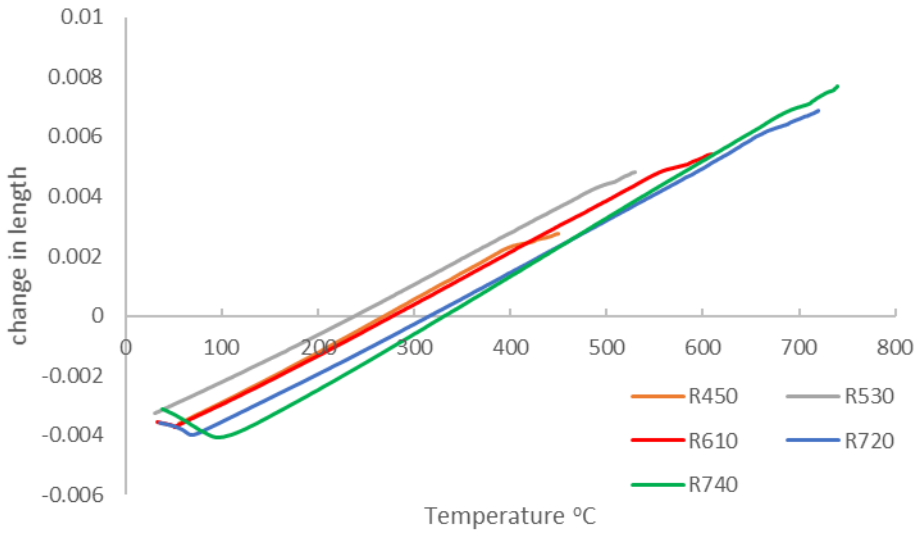

Figure 45 dilatometry cooling curve of reheated QP160. Legend is indicated on the graph.. Red arrow indicates the martensite formation upon quenching. It is observed on QPR610 (red line), QP160R720 (blue line) and QPR740 (green line)

The SEM pictures of all reheated QP160 samples are taken and analyzed. The samples are interrupted at 450 °C, 530 °C, 610°C, 720 °C, and 740°C of reheating temperature.

- Microstructure after reheating at 450°C

Figure 46 shows the SEM microstructures of QP160R450. Ellipsoid carbides are observed within M_1 matrix. Moreover, film type austenite and MA islands are also observed (Figure 46.b). The microstructure is similar to the microstructure of QP160 sample. Hence, it indicated that no microstructural events occurred after reheating up to 450°C.

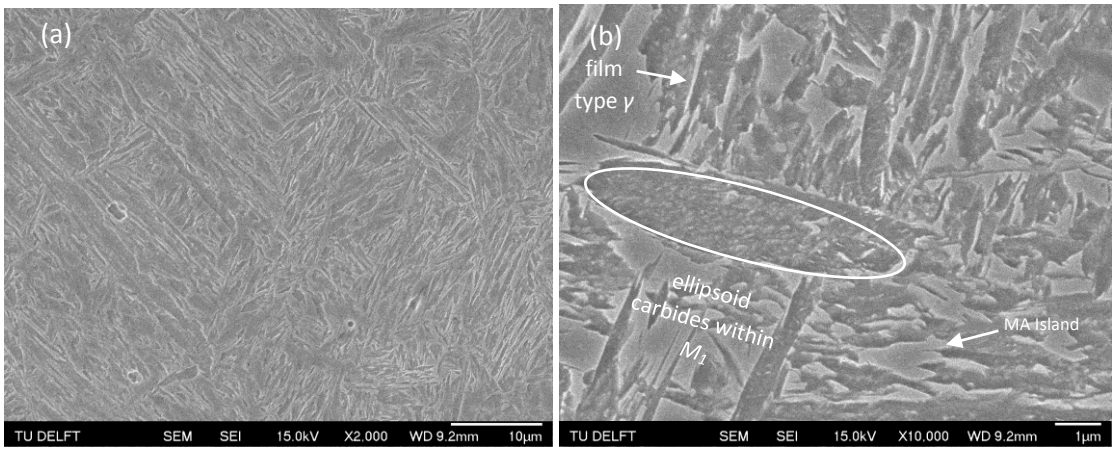

Figure 46 SEM pictures of QP160R450. (a) at 2000X magnification and (b) at 10.000X magnification. The white circles and arrows indicated the observed features on the microstructures

- Microstructure after reheating to 530ºC

Figure 47 shows the SEM microstructures of QP160R530. It can be seen that globular carbides, ellipsoid carbides, film type austenite and MA islands are spotted. The microstructures are not much changed comparing to QP160 sample even though globular carbides start to be found. Hence, the changes in slope between 470ºC and 540ºC cannot be explained yet.

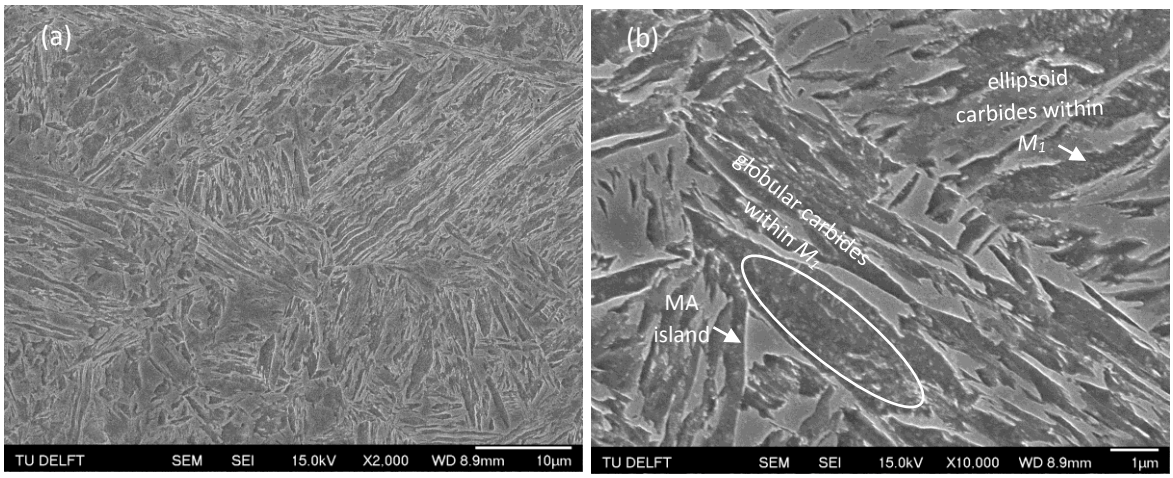

Figure 47 SEM pictures of QP160R530. (a) at 2000X magnification and (b) at 10.000X magnification. The white circles and arrows indicated the observed features on the microstructures

- Microstructure after reheating to 610ºC

Figure 48 shows the SEM microstructures of QP160R610 sample. In Figure 48 (b), several features are observed explaining the changes in slope between 470ºC and 540ºC. First, less ellipsoid carbides and more globular carbides are situated within M_1 matrix. Second, discrete particles of cementite are observed. Those are the decomposition product of film type retained austenite. Third, it is also found sub-grain structure or carbon depleted area within MA islands as a product of retained austenite decomposition.

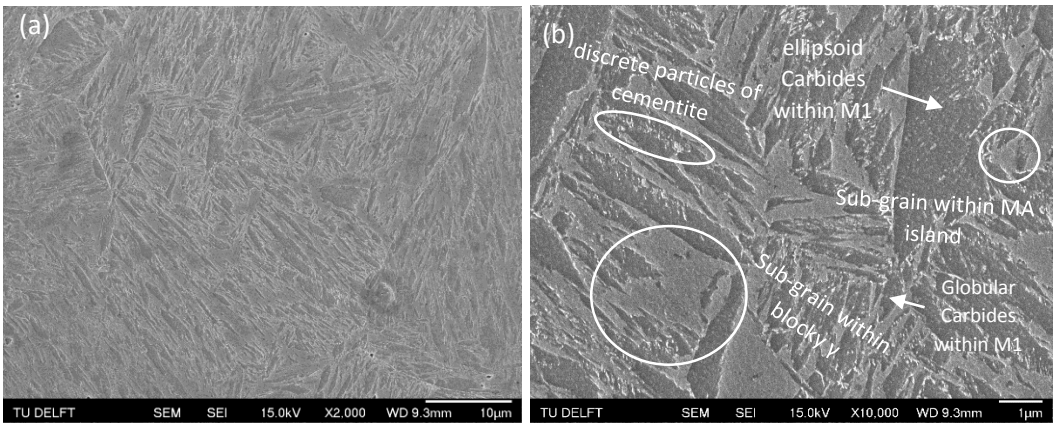

Figure 48 SEM pictures of QP160R610. (a) at 2000X magnification and (b) at 10.000X magnification. The white circles and arrows indicated the observed features on the microstructures

In summary, the observed features comparison in the microstructures of QP160R450, QP160R530, and QP160R610 samples can be found in Table 5.

The changes in slope between 470ºC and 540ºC cannot be explained by the QP80R450 and QP80R530 microstructures since they have similar features with QP160 sample. Prominent changes are observed in QP160R610, which has higher reheating temperature than the reheating temperature where a changes in slope observed. It indicates that microstructural events correspond to the changes in slope already ended after reheating to 610ºC. Therefore, the changes in slope between 470ºC and 540ºC can be explained by the formation of globular carbides, retained austenite decomposition into discrete particles of cementite, and formation of sub-grain structure within MA islands.

Table 5 The observed features comparison in microstructures of QP160450, QP160530, and QP160610

Samples	Features
QP80R450	Ellipsoid carbides can be found within M_1 matrix
	Film type austenite
	MA islands comprise of austenite surrounded M_2
QP80R530	Ellipsoid carbides can be found within M_1 matrix
	Globular carbides start to be detected
	Film type austenite
	MA islands comprise of austenite surrounded M_2
QP80R610	Ellipsoid carbides can be found within M_1 matrix. The amount of it is relatively similar which is found in QP80R450 and QP80R530
	Globular carbides are more dominant than the ellipsoid carbides
	Film type austenite. Some decompose into discrete particles of cementite

- Microstructure after reheating to 720ºC

Figure 49 shows the SEM microstructures of the QP160R720 sample. The globular carbides are observed within the M_1 matrix and MA islands. Moreover, discrete particles of cementite are also spotted. No sub-grain structure observed on the retained austenite grains or MA islands. Hence, the changes in slope between 690ºC and 720ºC correspond to the dissolution of ellipsoid carbide and formation of globular carbides.

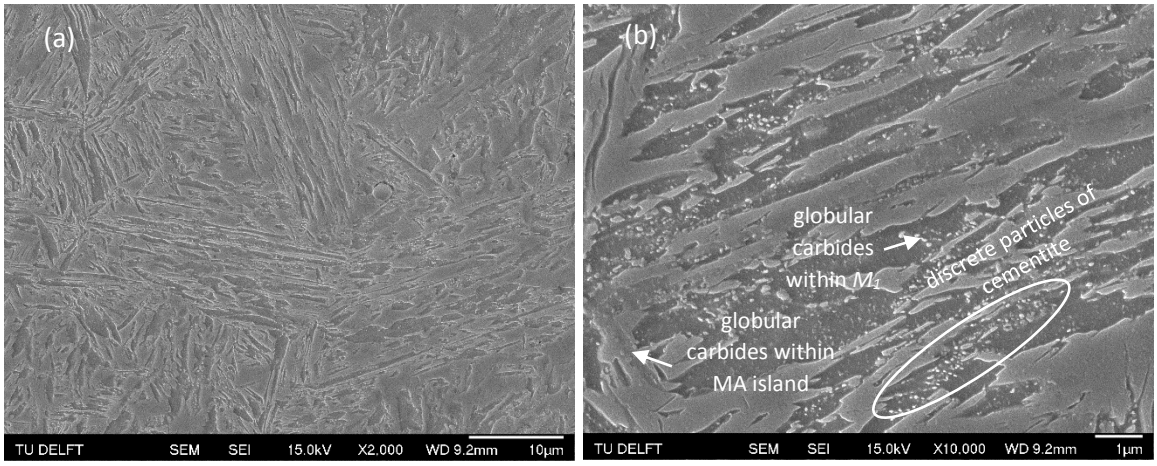

Figure 49 SEM pictures of QP160R720. (a) at 2000X magnification and (b) at 10.000X magnification. The white circles and arrows indicated the observed features on the microstructures

- Microstructure after reheating to 740°C

Figure 50 shows the optical microscopy microstructures of QP160R740 sample. The micrograph consists of the martensite region (dark region) surrounded by river-like pattern (light region) indicating by red arrows in Figure 50 (a). In Figure 50 (b), it revealed that lath martensite sits inside the river-like pattern, but it has different crystallographic direction compared with lath martensite situated alongside the river-like pattern.

Micro-hardness tests (0.05 kgf) are performed in order to clarify the phase of river-like patterns by comparing its hardness with the dark region. The river-like pattern shows 531.6 HV, which is higher than the dark region 491.4 HV. The difference in hardness is less compared to QP80R740 sample indicating both regions consist of similar constituent phases. The river-like pattern consist of martensite which originally came from new austenite as a product of (martensite and) carbide transformation and lath martensite which originally came from the unstable austenite forming upon reheating process (Figure 45). It can be said that the contraction between 720°C and 750°C is related to the formation of austenite.

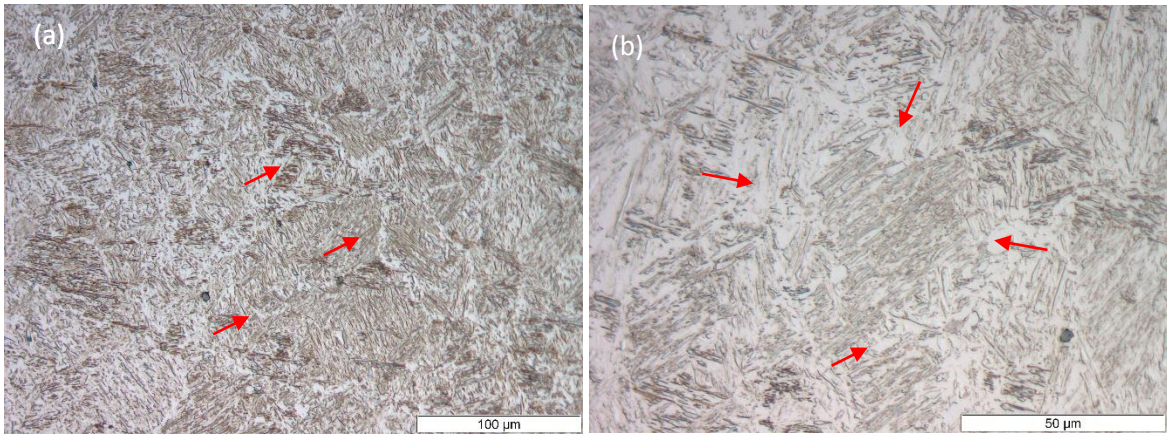

Figure 50 OM pictures of QP160R740. (a) at 20X magnification and (b) 50 X magnification. The red arrows indicated the river like pattern that surrounded martensite

The comparison between the microstructures of QP80R720 and QP80R740 samples can be found in Table 6.

Table 6 The observed features comparison in microstructures of QP160720 and QP160740

Samples	Observed features
QP160R720	Globular carbides can be found throughout the microstructures, namely within M_1 and austenite grain boundaries
	Discrete particles of cementite
QP160R740	River-like pattern consists of lath martensite which originally came from new austenite.

- X-Ray diffraction curve of the interrupted reheating QP80 samples

Figure 51 depicted the X-Ray Diffraction curve of the QP160 samples after subjected to interrupt reheating process. The austenite peaks, {111}, {200}, {220}, and {311} starts to decay after reheating at 610^{o}C and start to increase again after reheated at 720^{o}C and 740^{o}C. In the two latter cases, additional ferrite peaks observed and overlapped the existing one. Those can correspond to the formation of new martensite after quenching which originally came from new austenite.

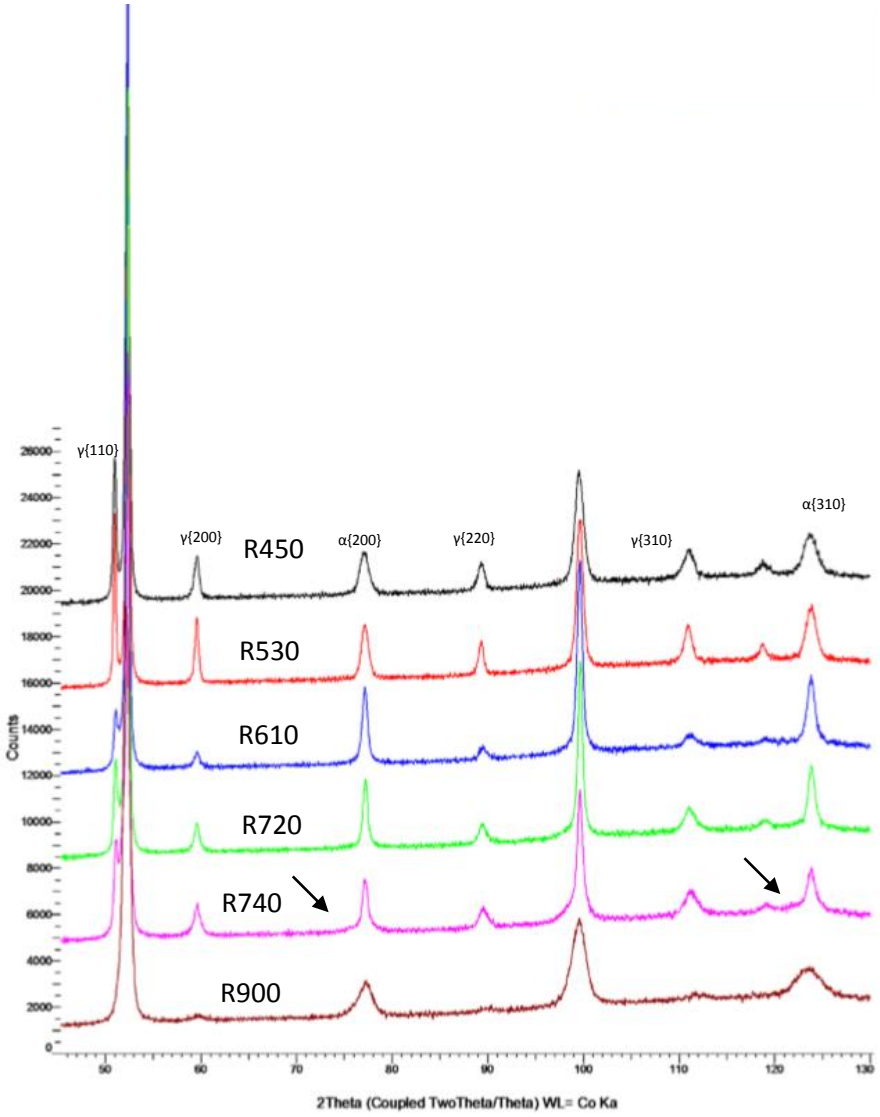

Figure 51 X-Ray Diffraction curve for QP160 after reheating up to 900°C. Black arrows are indicated the overlapping ferrite peaks

The evolution of f_{RA} during reheating process can be seen in Figure 52. It is observed that the specimen QP160 has relatively high f_{RA} which still remained up to 530°C of reheating temperature. Further reheating temperature beyond 610°C caused significant decreasing of f_{RA} which will hold up to 700°C. The significant decrease of retained austenite fraction can be described by the formation of the discrete particles of cementite coming from film type austenite and the formation of carbides within the M_1 matrix as described in Figure 48 and Table 5. On the other hand, the increased retained austenite fraction can be described by the formation of the new austenite as it confirmed by the presence of the lath martensite inside the river-like pattern in Figure 50(b).

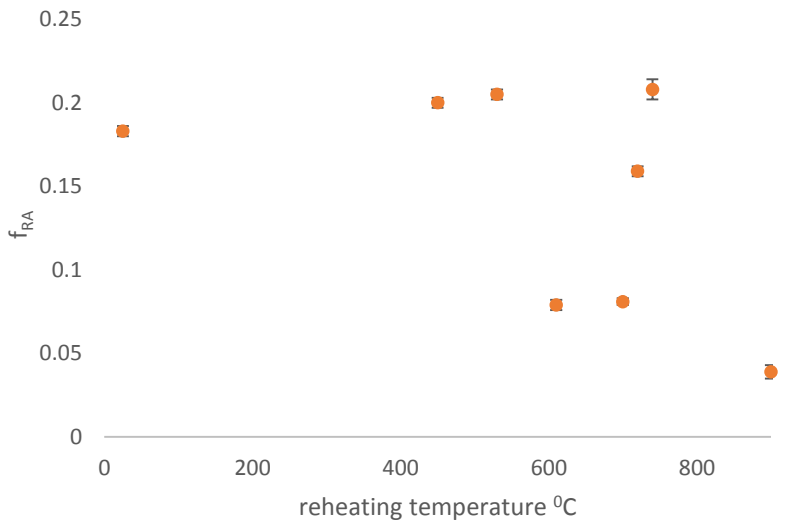

Figure 52 f_{RA} evolution of QP160 during reheating up to 900°C

- Summary: Reheating of QP160

Interrupted reheating treatments were applied to QP160 samples. The formation of globular carbides within the M_1 matrix, discrete particles of cementite from the film type austenite, and sub-structure within MA islands and blocky austenite are observed after QP160 samples reheated up to 610°C. Those are correlated with the change in slope between 470°C and 540°C in Figure 44. It might possibly explains the decrease in the retained austenite fraction into constant value after reheating process.

River-like structures surrounded martensite (dark) region are observed in QP160R740. The presence of lath martensite within the light region and the hardness value comparison indicated the formation of new austenite after QP160 sample reheated up to 740°C. It means that new austenite formation is correlated with the changes in slope between 720°C and 745°C

3.2.2.3 Comparison between QP80 and QP160

Figure 53 shows the retained austenite fraction evolution with respect to the reheating temperature. It shows that:

- At 450°C-530°C of reheating temperatures: the retained austenite has a good thermal stability indicating the alloy ability to preserve the retained austenite fraction that is produced after Q&P process.
- At 610°C-700°C of reheating temperatures: both QP80 and QP160 samples have a constant value of the retained austenite regardless of its reheating temperatures. It seems that they lost their stability and decomposed into ferrite and carbides in both cases. Retained austenite which has better thermal stability remains untransformed at higher reheating temperatures.

- There is a critical temperature of retained austenite decomposition approximately at 600°C (dashed line in Figure 53). Below the critical temperature, the f_{RA} is dependent on quenching temperature and can retain since they are carbon-rich after partitioning process
- At 720°C-740°C of reheating temperatures: As the temperature increased, the f_{RA} starts to grow at around 700°C of reheating temperature. The retained austenite fraction of both samples increase to the same value as the higher reheating temperature regardles its Q&P process. The f_{RA} at 900°C represented the retained austenite which not transformed into martensite upon quenching into room temperature.

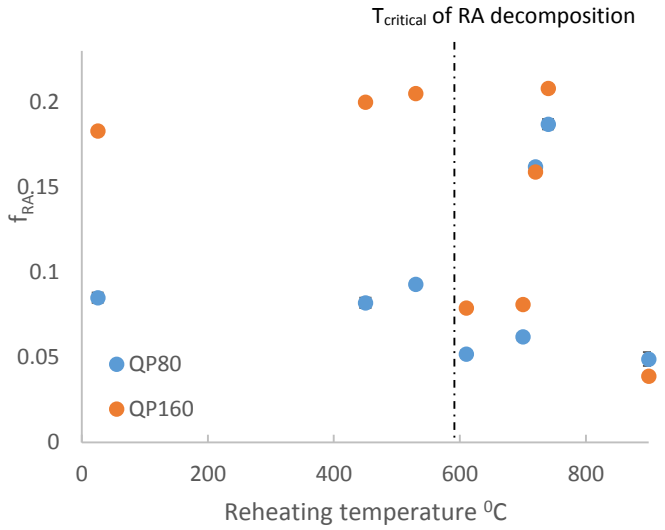

Figure 53 f_{RA} evolution of QP80 and QP160 during reheating up to 900°C. The dashed line indicates the assumed RA decomposition temperature

Figure 54 shows the comparison of QP80 and QP160 dilatometry curve when they are reheated followed by quenching to room temperature. It shows that:

- At the critical temperature of retained austenite decomposition (600°C): linear thermal expansion during reheating and linear thermal contraction during quenching indicating no microstructural events occurred. Moreover, the decomposition of retained austenite cannot be observed in the dilatometry curve.
- At 700°C – 800°C: An unusual anomaly at the onset of austenitization is observed on both curves.
- The M_s temperature of the reheated samples shifted to a higher temperature. It can be seen that the M_s temperature of QP80 shifted to the higher temperature (300°C) compare with QP160 (248°C) and un-reheated samples (approximately at 241°C).

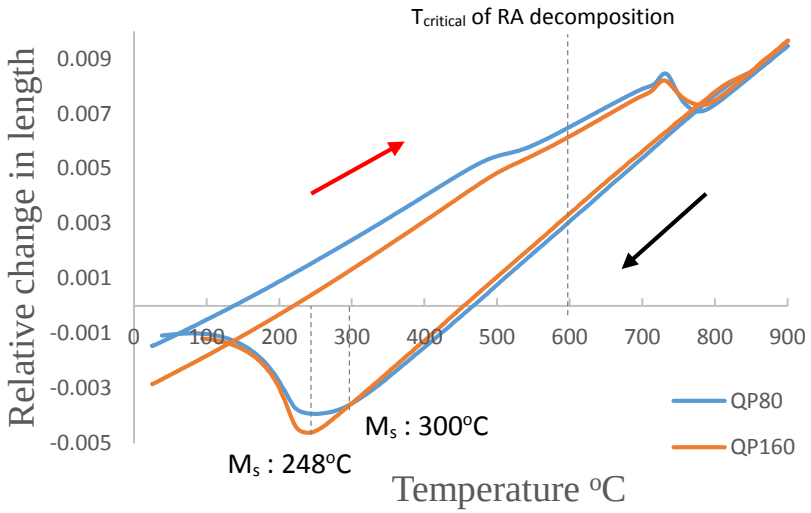

Figure 54 Dilatometry curve of reheated QP80 and QP160 followed by quenching to room temperature. The red arrow indicates reheating direction, whereas the black arrow indicates the quenching direction

3.2.2.4 Comparison with the equilibrium condition

The detailed analysis of the reheating process on the Q&P samples are discussed in the previous subsection (3.2.2.1-3.2.2.3). Figure 55 shows the equilibrium fractions of all phases including austenite (FCC), ferrite (BCC), and cementite (Fe_3C). Some remarks on the figure compare to the obtained observation are following:

- In the non-equilibrium condition above it is observed that the retained austenite decomposition can be captured at 450-600°C depending on the initial microstructure (Figure 37-41 for QP80 samples and Figure 46-50 for QP160 samples. In the equilibrium condition, austenite formation starts at A_1 temperature (710°C) meaning that the decomposition of retained austenite began earlier in non-equilibrium condition.
- In the non-equilibrium condition, cementite starts to be observed at samples reheated up to 610°C lower which another type of carbides is present. In the equilibrium condition, cementite is present from 200-680°C in the equilibrium calculation. It means that the cementite formation is delayed compared with equilibrium condition
- In the non-equilibrium condition, austenitization starts from 690-700°C and finished at 800°C (Figure 35.a and Figure 44.a). In the equilibrium condition, austenitization starts from 600°C and finished at 740°C. It means that the martensite reversion is delayed in the non-equilibrium condition

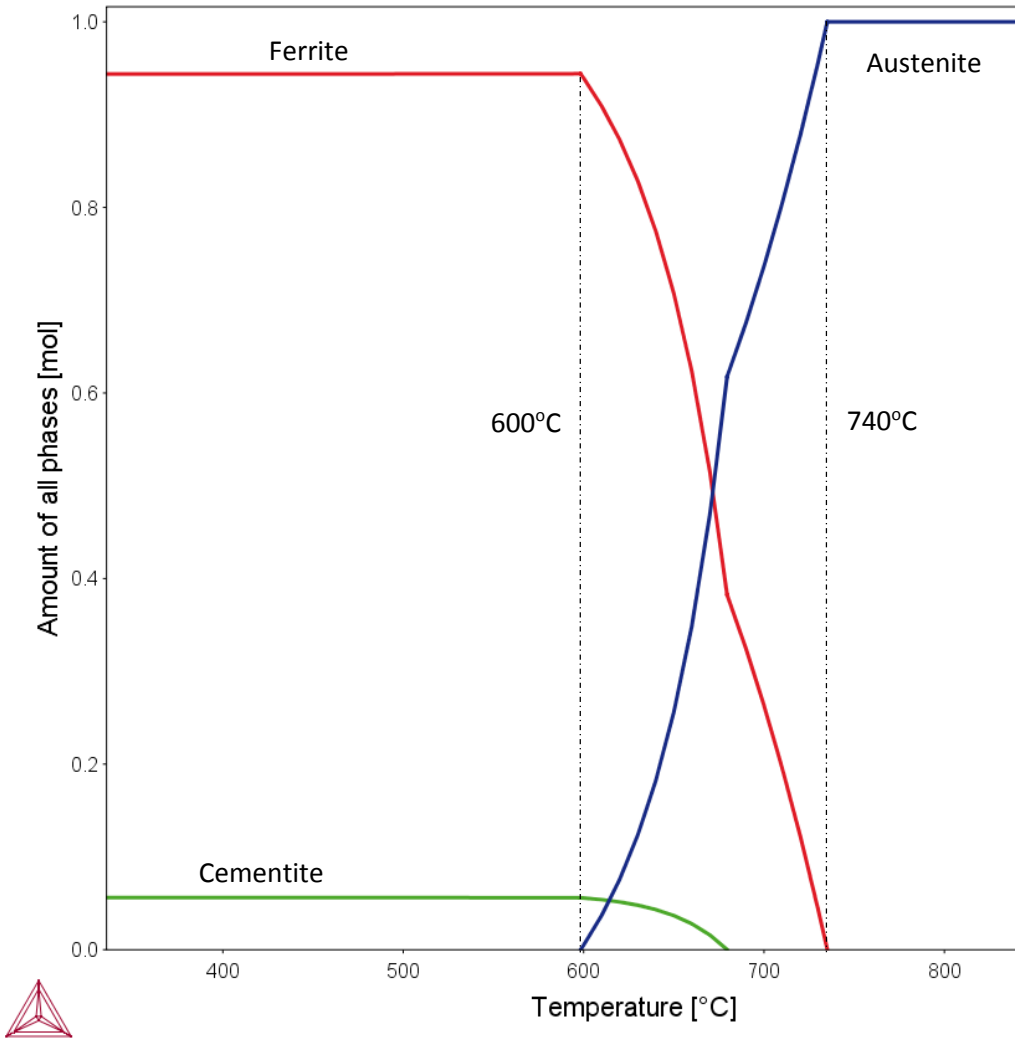

Figure 55 Evolution of the equilibrium phase fraction as the temperature increases. Calculated by Thermocalc. The phases are indicated on the graph

Chapter 4: Conclusion and recommendations

4.1 Conclusions

A Q&P steel with chemical composition 0.33C-4.58Mn-1.98Si (wt.%) is subjected to Quenching and Partitioning (Q&P) heat treatments with different quenching temperatures (from 80-260ºC) and constant partitioning conditions (400ºC and 50 s), followed by reheating treatments at elevated temperature. It is found that after reheating to 700ºC and followed by quenching to room temperature, the volume fraction of retained austenite tended to similar values (0.05-0.08) regardless of the quenching temperature. In order to study this phenomenon, two samples subjected to Q&P process with different quenching temperature (80ºC and 160ºC) are reheated up to 900ºC. These samples represented the smallest and highest drop of retained austenite fraction after reheating to 700ºC.

The microstructural events during the reheating process are observed by means of dilatometry. There are three peaks in derivative of dilatometry curve at approximately 530ºC, 720ºC, and 740ºC. Interrupted reheating processes followed by quenching to room temperature are applied on both specimens near the observed peaks. Hence, the samples are reheated at 450ºC, 530ºC, 610ºC, 720ºC, and 740ºC. The microstructure and retained austenite fraction are taken and measured to describe the microstructural events that happened during reheating followed by quenching into room temperature. Several conclusions can be drawn, namely:

- Reheating of QP80 sample

Regarding the changes in slope between 470ºC and 530ºC, the decomposition of retained austenite can be described with two mechanisms, namely: formation of discrete particles of cementite in former austenite and formation of globular carbides within tempered martensite matrix. The first case is detected after the samples are reheated up to 450ºC and higher. The discrete particles of cementite came from the film type retained austenite. In the second case, the globular carbides, which were found after reheating up to 610ºC, replaced the ellipsoid carbides, which were already found since the samples reheated up to 450ºC.

Regarding formation of austenite, it occurred in three consecutive microstructural events, namely: the dissolution of remaining ellipsoid carbides and formation of more globular carbides correlated with the changes in slope between 700ºC and 720ºC of reheating temperature, (martensite and) carbide to austenite transformation characterized by an expansion between 720ºC and 750ºC, and further formation of austenite characterized by a large contraction between 750ºC and 800ºC.

The river-like patterns, were observed after samples reheated up to 740ºC, surrounded the dark regions. The closer look into the river-like pattern showed that it did not contain other features except the etched

light region. The micro hardness test showed that the river-like pattern mainly consists of martensite from the (martensite and) carbide to austenite transformation.

- Reheating of QP160 samples

Regarding the changes in slope between 470°C and 580°C, the decomposition of retained austenite can be described with three mechanisms, namely: the formation of discrete particles of cementite, the formation of substructure within MA islands, and the formation of globular carbides. The first two mechanisms took place after the samples are reheated up to 610°C or higher. The globular carbides were already observed after the samples were reheated up to 530°C or higher.

Regarding the formation of austenite, it occurred in three consecutive microstructural events, namely: the dissolution of remaining ellipsoid carbides and formation of more globular carbides correlated with the changes in slope between 690°C and 720°C of reheating temperature, (martensite and) carbide to austenite transformation characterized by an expansion between 720°C and 745°C, and further formation of austenite characterized by a large contraction between 745°C and 800°C.

The river-like patterns observed after the samples are reheated up to 740°C. It surrounded lath martensite region (dark region). The micro-hardness test showed that the river-like pattern consist of similar constituent phases like the dark region, namely: martensite which originally came from new austenite as a product of (martensite and) carbide transformation and lath martensite which originally came from the unstable austenite forming upon reheating process

- Retained austenite fraction evolution on QP80 and QP160

By comparing the retained austenite fraction evolution, it is examined that there is a critical retained austenite decomposition temperature upper which caused the decreased of the retained austenite fraction into constant value regardless of its quenching temperature. The critical retained austenite decomposition temperature for current Q&P steel is approximately at 600°C.

- Comparison with the equilibrium condition

It has been discussed that the retained austenite decomposition began earlier in non-equilibrium condition, whereas cementite formation and martensite reversion are delayed in non-equilibrium condition.

4.2 Recommendations

1. Verification on the decomposition mechanisms is recommended. In-situ reheating testing can be described and tracked the decomposition mechanisms. Another suggestion is by developing a simulation of the decomposition of retained austenite in Q&P steel during reheating.

2. Verification on the decomposition products is suggested. For example, characterization of carbides can be done by TEM analysis in order to study carbides type observed in the current study. Its crystal structure, crystallographic orientation, morphology, etc can give a comprehensive understanding on the thermal stability of the retained austenite
3. Reheating at different heating rates can be done in order to calculate the activation energy of each microstructural events. Carbides formation, for instance. By calculating the activation energy, the corresponding microstructural event can be correlated with other phenomena which have a similar value of activation energy.
4. The increase of the retained austenite fraction on some samples during reheating is an interesting point to study. This can be useful to get an explanation on how the Q&P steel can be softened upon reheating.

Chapter 5: References

[1] T. Koopmans, "Thermal stability of retained austenite in Quenching & Partitioning steels - Master Thesis," Department of Materials Science and Engineering at the Delft University, Delft, 2015.

[2] D. Matlock, J. Speer, E. De Moor and P. Gibbs, "Recent developments in advanced high strength sheet steel for automotive applications: an overview," *Jestech,* vol. 15, no. 1, pp. 1-12, 2012.

[3] Worldautosteel, "worldautosteel.org," [Online]. Available: http://www.worldautosteel.org/wp-content/uploads/2012/03/AHSSDiagram_WorldAutoSteel-copy.png. [Accessed 26 3 2018].

[4] J. Speer, D. Matlock, B. De Cooman and J. Schroth, "Carbon partitioning into austenite after martensite transformation," *Acta Materialia,* vol. 51, no. 9, p. 2611–2622, May 2003.

[5] J. Speer, F. Assuncao, D. Matlock and Edmonds, D.V, "The 'quenching and partitioning' process: background and recent progress," *Materials Research,* vol. 8, no. 4, p. 417–423, Dec. 2005.

[6] B. Kim, J. Sietsma and M. Santofimia, "The role of silicon in carbon partitioning processes in martensite/austenite microstructures," *Materials & Design,* vol. 127, p. 336–345, Aug. 2017.

[7] A. J. Clarke, J. Speer, D. Matlock , F. Rizzo, D. Edmonds and M. Santofimia, "Influence of carbon partitioning kinetics on final austenite fraction during quenching and partitioning," *Scripta Materialia,* Vols. 61, no. 2, p. 149–152, Jul. 2009.

[8] M. Hillert and J. Agren , "Reply to comments on 'On the definition of paraequilibrium and orthoequilibrium'," *Scripta Materialia,* vol. 52, pp. 87-88, 2005.

[9] N. Zhong, X. Wang, Y. Rong and L. Wang, "Interface Migration between Martensite and Austenite," *Journal of materials science and tenchnology,* vol. 22, no. 6, p. 751, 2006.

[10] M. J. Santofimia , L. Zhao and J. Sietsma, "Model for the interaction between interface migration and carbon diffusion during annealing of martensite–austenite microstructure in steels," *Scripta Materialia,* vol. 59, pp. 159-162, 2008.

[11] M. J. Santofimia , L. Zhao and J. Sietsma , "Microstructural Evolution of a Low-Carbon Steel during Application of Quenching and Partitioning Heat Treatments after Partial Austenitization," *Metallurgical and Materials Transactions A,* Vols. vol. 40, no. 1,, p. 46–57, Nov. 2008.

[12] P. Morra, A. Bottger and E. Mittemeijer, "Decomposition of iron-based martensite. A kinetic analysis by means of differential scanning calorimetry and dilatometry," *Journal of Thermal Analysis and Calorimetry,* vol. 64, pp. 905-914, 2001.

[13] J. Mola and D. C. Bruno , "Quenching and Partitioning (Q&P) Processing of Martensitic Stainless Steels," *Metallurgical and Materials Transactions A,* vol. 44, no. 2, pp. 946-967, 2012.

[14] A. J. Kolk, "Is retained austenite controlling the mechanical properties of Q&P steels ? - Master Thesis," Department of Materials Science and Engineering at the Delft University, Delft, 2014.

[15] S. van der Zwaag, L. Zhao, S. Kruijver and J. Sietsma, "Thermal and Mechanical Stability of Retained Austenite in Aluminum-containing Multiphase TRIP steels," *ISIJ International,* vol. 42, no. 12, pp. 1565-1570, 2002.

[16] L. Samuels , "Tempering of Martensite," *Metallography, Microstructure, and Analysis, ,* vol. 3, no. 1, pp. 70-90, 2014.

[17] G. Krauss, "Tempering of Martensite," *Reference Module in Materials Science and Materials Engineering,* 2016.

[18] H. Badheshia and R. Honeycombe, "Tempering of Martensite," in *Steels: Microstructures and Properties*, Cambridge, Elsevier Ltd, 2017.

[19] K. He, D. Edmonds, J. Speer, D. Matlock and F. Rizzo, "Martensite tempering behaviour relevant to the quenching and partitioning process," *Materials Science ,* vol. 2, pp. 431-432, 2008.

[20] E. de Moor , C. Fojer , J. Penning , A. Clarke and J. Speer, "Calorimetric study of carbon partitioning from martensite into austenite," *Physical Review B,* vol. 82, 2010.

[21] R. Wu, L. Wang and X. Jin, "Thermal Stability of Austenite and Properties of Quenching & Partitioning (Q&P) Treated AHSS," *Physics Procedia,* vol. 50, pp. 8-12, 2013.

[22] E. de Moor, S. Lacroix, L. Samek, J. Penning and J. Speer, "Dilatometric Study of the Quench and Partitioning Process," in *The 3rd International Conference on Advanced Structural Steels*, Gyeongju, 2006.

[23] ASM International , "Introduction to Steels and Cast Irons," in *Metallographer`s Guide: Irons and Steels* , Ohio, 2002, p. 2.

[24] M. J. Santofimia, L. Zhao, R. Petrov, C. Kwakernaak, W. Sloof and J. Sietsma, "Microstructural development during the quenching and partitioning process in a newly designed low-carbon steel," *Acta Materialia,* vol. 59, no. 15, pp. 6059-6068`, 2011.

[25] G. Krauss, "Solidification, segregation, and banding in carbon and alloy steels," *Metallurgical and Materials Transactions B,* vol. 34, no. 6, pp. 781-792, 2003.

[26] G. v. Voort, "Microstructure," in *Metallography, principles and practice*, New York, USA, ASM International, 1999, p. 167.

[27] T. A. Kop, J. Sietsma and S. van der Zwaag , "Dilatometric analysis of phase transformations in hypo-eutectoid steels," *Journal of Materials Science,* vol. 36, pp. 519-526, 2001.

[28] T. N. Minh, "Quenching and PArtitioning of low alloyed steels ; Master Thesis," TU Delft, Delft, 2008.

[29] H. Bhadeshia and H. Honeycombe, "Bainite," in *Steels: Microstructure and Properties* , Elsevier Ltd., 2017, pp. 192-193.

[30] R. Huizenga , "XRD analysis of steel samples: calculating (retained) austenite fraction," Materials Science and Engineering department , TU Delft, DElft, 2018 .

[31] C. Jatczak, J. Larson and S. Shin, "Retained Austenite and its Measurements by X-ray Diffraction," *Society of Automotive Engineers Inc,* p. 9, 1980.

[32] R. Huizenga , "XRD analysis of steel samples: Lattice parameter of austenite," Department of materials science and engineering, TU Delft , Delft, 2018.

[33] J. Dossett and H. Boyer, "Fundamentals of the Heat Treating of Steel," in *Practical Heat Treating: Second Edition*, Ohio, ASM International, 2006, p. 22.

[34] H. Badheshia and M. Peet, “www.phase-trans.msm.cam.ac.uk,” University of Cambridge, [Online]. Available: https://www.phase-trans.msm.cam.ac.uk/map/steel/programs/mucg83.html#desc. [Accessed 15 October 2017].

[35] S. van Bohemen , "Bainite and martensite start temperature calculated with exponential carbon dependence," *Material Science Technology ,* vol. 28, no. 4, pp. 487-495, 2012.

[36] S. van Bohemen and J. Sietsma, "Effect of composition on kinetics of athermal martensite formation in plain carbon steels," *Materials Science and Technology,* vol. 25, no. 6, p. 1009–1012, 2009.

[37] G. Ramesh and N. Prabhu, "Review of thermo-physical properties, wetting and heat transfer characteristics of nanofluids and their applicability in industrial quench heat treatment," *Nanoscale Research Letters,* vol. 6, p. 334, 2011.

[38] L. Cheng, C. Brakman, B. Korevaar and E. Mittemeijer, "The Tempering of Iron-Carbon Martensite; Dilatometric and Calorimetric Analysis," *Metallurgical Transactions A,* vol. 19A, pp. 1988--2415, 1987.

[39] C. Garcia de Andres , F. Caballero and C. Capdevila , "Dilatometric Characterization of Pearlite Dissolution in 0.1C-0.5Mn Low Carbon Low Manganese Steel," *Scripta Materialia,* vol. 38, no. 12, pp. 1835-1842, 1998.